Received: 28 May 2025 | Revised: 22 July 2025 | Accepted: 25 July 2025

DOI: 10.1002/pro.70258

RESEARCH ARTICLE

THE PROTEIN SOCIETY WILEY

Unraveling ShuA detergent-induced colloidal behavior in solution: A comprehensive SEC-MALS, SAXS, and SANS study

A. Pozza[1] | A. Martel[2] | M. Moir[3] | T. A. Darwish[3] | K. Wimalan[4] | A. Koutsioubas[5] | S. Combet[4] | F. Bonneté[1]

[1]Université Paris Cité, CNRS, Laboratoire de Biochimie des Protéines Membranaires, Institut de Biologie Physico-Chimique, Paris, France

[2]Large Scale Structures, ILL Neutrons for Society, Institute Laue-Langevin, Grenoble, France

[3]National Deuteration Facility (NDF), Australian Nuclear Science and Technology Organization (ANSTO), Lucas Heights, New South Wales, Australia

[4]Laboratoire Léon-Brillouin, UMR12 CEA, CNRS, Université Paris-Saclay, Gif-sur-Yvette, France

[5]Jülich Centre for Neutron Science at Heinz Maier-Leibnitz Zentrum (MLZ), Forschungszentrum Jülich, Garching, Germany

Correspondence
A. Pozza and F. Bonneté, Université Paris Cité, CNRS, Laboratoire de Biochimie des Protéines Membranaires, Institut de Biologie Physico-Chimique, Paris, France.
Email: pozza@ibpc.fr and francoise.bonnete@ibpc.fr

Funding information
LABEX DYNAMO, Grant/Award Number: ANR-11-LABX 0011; CNRS-MITI interdisciplinary program "Modélisation du vivant"

Review Editor: Aitziber L. Cortajarena

Abstract

In this study, we investigate the detergent-induced behavior of the integral membrane protein ShuA in solution, focusing on its interactions with octyl polyoxyethylene (OPOE) and *n*-dodecyl-β-D-maltoside (DDM). Using a combination of size-exclusion chromatography coupled with multi-angle light scattering (SEC-MALS) and small-angle scattering techniques (SAXS and SANS), we provide a detailed characterization of the protein–detergent complex (PDC) behavior under varying conditions. Our results reveal that ShuA remains monomeric in 1% OPOE, whereas in 0.5 mM DDM, it undergoes a reversible monomer/dimer equilibrium that shifts towards a monodisperse, monomeric state with increasing DDM concentration to 7.5 mM, highlighting the significant influence of detergent type and concentration on protein colloidal stability. These findings have direct implications for membrane protein purification and structural studies, particularly in crystallization and cryo-EM sample preparation. The study emphasizes the necessity of optimizing detergent conditions to ensure monodispersity and structural integrity, preventing detergent-induced artifacts that could affect structural interpretations. Importantly, our results highlight the power of the SEC-MALS technique in determining oligomeric or association equilibrium states, detecting weak intermolecular interactions often overlooked in conventional SEC, and achieving this even in the particularly complex case of MPs. By integrating advanced scattering techniques, this work contributes valuable insights into MP colloidal behavior, refining strategies for structural characterization and providing a framework for optimizing detergent conditions in biochemical and biophysical studies.

KEYWORDS
colloidal interactions, crystallization, detergent, light scattering, membrane protein, oligomerization, size-exclusion chromatography, small-angle X-ray and neutron scattering

1 | INTRODUCTION

Membrane proteins (MPs) play crucial roles in cells, acting as receptors for external signals, transporters of ions and molecules across the membrane, and performing other vital functions. Their involvement in various diseases makes them important drug targets (Yin & Flynn, 2016). Consequently, an in-depth understanding of their structure–function relationship is essential for developing new therapeutic treatments.

Over the last few decades, research on MPs has made significant progress, thanks to advances in technologies and methodologies, particularly in crystallography (XRD), cryo-electron microscopy (cryo-EM), computational methods and machine learning (Birch et al., 2020; Chien et al., 2025; Guan, 2023; Healey et al., 2021; Sun et al., 2023). This progress is reflected in the explosion of unique structures in the "MPs of Known 3D Structure" database (https://blanco.biomol.uci.edu/mpstruc/), which grew more than tenfold, from 176 structures in 2007 to 1857 in 2024. Despite these successes, the study of MPs remains challenging, primarily due to difficulties in sample preparation, which range from the expression of the protein gene in homologous or heterologous systems to the solubilization of the host lipid membrane and the purification of the protein using appropriate amphiphilic molecules (usually detergents). Furthermore, maintaining the long-term stability of purified membrane protein–amphiphile complexes for biophysical and structural studies is a remaining issue.

A critical factor in sample preparation is the selection of detergent molecules used during the purification process. The nature of the detergent (non-ionic, ionic, and zwitterionic) is crucial as it can influence the stability and proper folding of the MP (Pocanschi & Kleinschmidt, 2022; Tulumello & Deber, 2012). Despite some attempts at rationalizing detergent selection (Newstead et al., 2008; Urner et al., 2023; Yoon et al., 2024), there is no standardized approach, while the physico-chemical interactions between detergents and MPs may provide useful insights into sample preparation or potentially explain unexpected results. Among the standard detergents used, and despite the use of protocols and commercial screens to identify optimal detergents or the synthesis of newer detergent and non-detergent molecules, *n*-dodecyl-β-D-maltoside (DDM), *n*-decyl-β-D-maltoside (DM), and *n*-octyl-β-D-glucoside (OG) remain among the most widely used for protein extraction, purification, and structural studies (Choy et al., 2021; Stetsenko & Guskov, 2017). Due to its low critical micelle concentration (CMC < 0.01%) and its low cost, DDM is often considered the gold standard in biochemistry and structural biology of MPs. While it is extensively used for solubilization (accounting for over 80% of total maltoside usage), its use in structural analysis depends on the method used to solve the protein structures. For example, when structures are determined using X-ray crystallography from in surfo crystals (i.e., in surfactant micelles), it may be beneficial to exchange long-chain detergents for short-chain detergents to form smaller detergent micelles around the hydrophobic transmembrane domain, thus allowing crystal contacts between hydrophilic domains of MP, particularly in the case of integral membrane proteins (IMPs). However, this may be at the expense of protein stability. Indeed, short-chain detergents (C7–C10) have been shown to destabilize or inactivate MPs (Lee et al., 2016), whereas long-chain detergents (C12–C14) are better suited to accommodate the protein hydrophobic domain, thereby maintaining its structure and function (Tate, 2010). Whether long- or short-chain detergents, with sugar-based (mono or di-glycoside) or poly(ethylene glycol)-based head groups, MPs are not always stable and functional in detergents. It is well known that a solution of MPs in detergents is complex, consisting of free detergent molecules, detergent micelles, and MPs embedded in a detergent belt (PDCs). Detergents can induce conformational changes, oligomerization, or aggregation through specific interactions with flexible protein regions (Yang et al., 2014), or non-specific interactions between detergent micelles and PDCs. To address these issues, extensive efforts have been made over several decades to develop new stabilizing surfactants and membrane-mimetic systems (Woubshete et al., 2024; Yoon et al., 2024). However, less attention has been given to understanding the effects of detergent micelles on the behavior of PDCs in solution, especially during sample preparation for structural studies such as crystallization screens or cryo-EM grid preparation. The oligomeric state of MPs, which is crucial for their stability and physiological function, can be altered during solubilization or purification, especially when detergents are used at high concentrations (Breyton et al., 1997) or when different detergents are applied (Fisher et al., 2003; Guo, 2020). However, distinguishing between MP oligomers embedded in detergent micelles and oligomers of PDCs can be challenging (Heuberger et al., 2002). Controlling the structure of MPs in detergent is key for preparing suitable samples for functional and structural studies. While the influence of detergents on the colloidal behavior of PDCs is often overlooked, these phenomena are well-studied in the context of nanoparticles for industrial applications such as drug delivery and cosmetics (Ray et al., 2018). Understanding these effects in the context of MP could help improve sample preparation for structural studies.

To describe the behavior of MPs in detergent solutions, scattering techniques such as multi-angle light scattering (MALS), small-angle X-ray scattering (SAXS), and small-angle neutron scattering (SANS) are particularly useful. When coupled in-line with size-exclusion chromatography (SEC), these methods offer valuable insights into the structure of macromolecules in heterogeneous solutions, as it is the case of membrane proteins in detergent solutions. SEC-MALS, which requires lower sample concentrations than SAXS or SANS and is thus considered a "dilute-regime" technique, allows direct determination of the molecular

weight of macromolecules in solution, making it particularly useful for monitoring oligomerization or polydispersity. SEC-SAXS and SEC-SANS, on the other hand, provide low-resolution structural information in dilute solutions—such as the overall shape and size of complexes—and are especially powerful in semi-dilute and concentrated solutions, where weak intermolecular interactions can be probed through structure factor analysis (Spinozzi et al., 2002; Zhang et al., 2007).

Although SAXS and SANS provide similar structural information, they present distinct advantages and constraints. SAXS, performed at synchrotrons, benefits from high flux and shorter measurement times, but can suffer from radiation damage. In contrast, SANS is free from radiation-induced artifacts and uniquely enables contrast variation by replacing hydrogen with deuterium, allowing selective visualization of specific components of the complex. This makes SANS particularly powerful when using deuterated detergents and D_2O-based buffers, as the detergent signal can be matched out to isolate the scattering from the protein alone (Combet et al., 2023; Midtgaard et al., 2018). However, the lower neutron flux requires higher sample concentrations, larger volumes, and longer exposure times compared to synchrotron SAXS. Additionally, replacing H_2O with D_2O in sample buffers can improve the signal-to-noise ratio in SANS measurements, but this substitution may also promote protein aggregation, even as it enhances conformational stability (Giubertoni et al., 2023; Reslan & Kayser, 2018). These effects are primarily due to increased hydrophobic interactions and the strengthening of intra- and intermolecular bonds resulting from hydrogen–deuterium exchange (Haidar & Konermann, 2023).

Despite their respective limitations, both techniques are further enhanced by computational modeling tools. Several software programs enable the ab initio reconstruction of biomolecules from 1D scattering data, including DAMMIF/N, MONSA, and DENFERT (Franke & Svergun, 2009; Koutsioubas et al., 2016; Molodenskiy et al., 2020; Svergun, 1999). These programs use collections of beads or dummy atoms, which are arranged in a shape that best fits the scattering profile of the biomolecule. A more recent approach (DENSS) directly calculates electron density maps from the SANS data (Grant, 2018; Sumner & Qian, 2022), without relying on predefined models or shapes, offering a more realistic 3D view of macromolecules, even complexes, in solution.

Other approaches enable modeling the detergent belt around a MP of known structure. For example, MemProt (Perez & Koutsioubas, 2015) uses a collection of dummy beads to generate a coarse-grained model by fitting an experimental SAXS curve knowing the MP all-atom 3D-structure. To expand MemProt's applicability to a wider range of detergents and belt geometries, Combet and collaborators are developing SASbelt, a new Python-based implementation (to be published) that adds a graphical interface, automated MP orientation, and a webserver dashboard (https://llb.cnrs.fr/sasbelt/). In addition, the Det.belt server (Zampieri et al., 2021) approximates the detergent belt as a hollow cylinder, based solely on the number of detergent molecules surrounding the MP. Although schematic, these representations of PDCs provide biochemists with valuable visual insights into their samples.

Analytical modeling using SasView (http://www.sasview.org/) can also be performed on 1D-scattering data to describe the geometry of the protein (Cleveland et al., 2018). All these modeling approaches can thus provide insights into the structure and spatial arrangement of protein assemblies or complexes in solution.

As a rule of thumb, structural studies using XRD or cryo-EM require pure, monodisperse samples that remain structurally stable during crystallization or grid preparation for successful results, even though cryo-EM is more tolerant in terms of sample quality, as small amounts of impurities do not prevent structure determination (García-Nafría & Tate, 2021). The behavior of PDCs in terms of oligomeric state and protein-bound detergent amount depends on the protein concentration but also on the type and concentration of detergent. In a previous study, we performed molecular modeling of ShuA in DDM by combining SEC-SAXS, SEC-MALS, and molecular dynamics (MD) simulations (Abel et al., 2021). ShuA, a 70 kDa TonB-dependent receptor from the outer membrane of *Shigella dysenteriae*, was crystallized in OG (Brillet et al., 2009), a detergent commonly used for β-barrel MPs due to its ability to form small micelles, thus allowing crystal contacts and crystal growth. The high-resolution structure of ShuA was solved at 2.6 Å by X-ray diffraction (PDB code: 3FHH), revealing a monomeric MP composed of 22 β-strands (Cobessi et al., 2010). Although the SEC-MALS profile revealed a polydisperse population of ShuA in DDM—comprising both monomeric ShuA–DDM complexes and higher molecular-weight species—we were able to model the DDM belt around ShuA using the atomic 3D structure (Abel et al., 2021). However, the origin of the heterogeneity observed in DDM remained unclear, whether the higher molecular-weight species represented oligomers of the ShuA–DDM complex or oligomers (e.g., dimers or trimers) of ShuA embedded in a DDM belt.

In the present study, we re-examine the behavior of ShuA in DDM and compare the results to those obtained using OPOE, the detergent originally used to solubilize and purify the protein from the outer membrane. ShuA was studied at concentrations ranging from 0.1 to 10 mg/mL using SEC-MALS and SEC-SAXS techniques. Additionally, SANS experiments were conducted to further elucidate the specific behavior of ShuA in the matched-out DDM solution. By

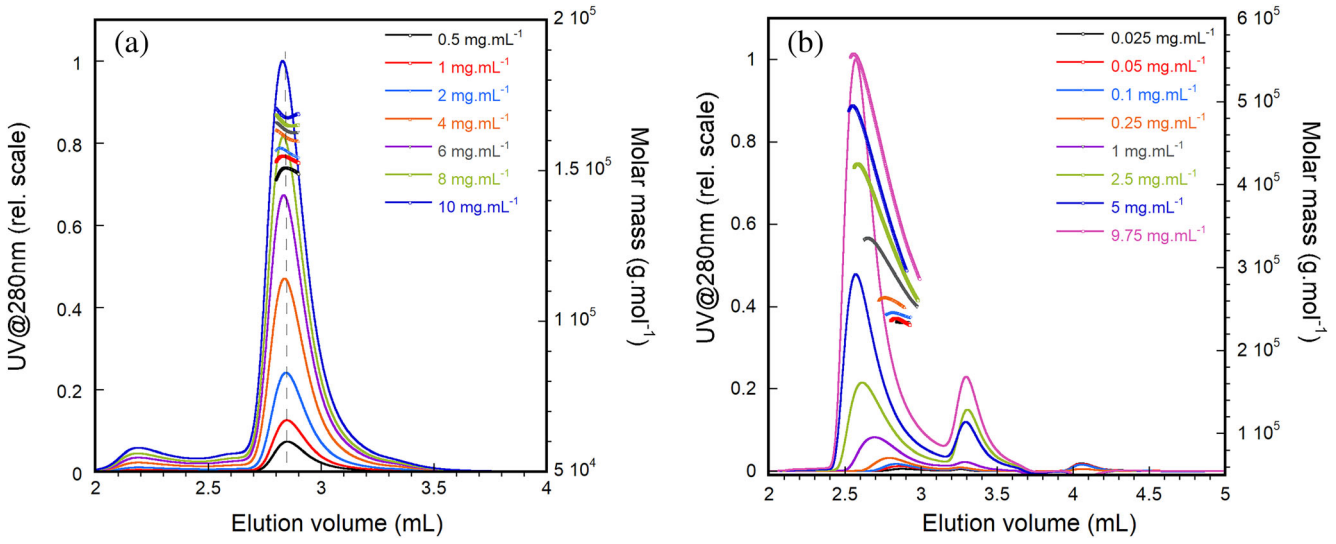

FIGURE 1 (a) SEC-MALS elution profiles of ShuA–OPOE, 20 μL injected between 0.5 and 10 mg/mL in 1% OPOE-containing buffer, eluted on a silica-gel column (BioZen, Phenomenex) at a flowrate of 300 μL/min, with 50 mM Tris–HCl pH 7.5, 150 mM NaCl, 1 mM EDTA, 1% OPOE: UV absorbance at 280 nm in solid line; symbols represent the calculated apparent molar masses for the protein–detergent complex at the different concentrations injected. (b) SEC-MALS elution profiles of ShuA–DDM, 20 μL injected between 0.025 and 9.75 mg/mL in 0.5 mM DDM-containing buffer, eluted on a silica-gel column (BioZen) at a flowrate of 300 μL/min, with 20 mM Tris–HCl pH 7.5, 100 mM NaCl, 1 mM EDTA, 0.5 mM DDM: UV absorbance at 280 nm in solid line; symbols represent the calculated apparent molar masses for the protein–detergent complex at the different concentrations injected.

analyzing the distinct behaviors of ShuA in OPOE and DDM, we were able to explain its dimer formation and subsequently optimize its crystallization in DDM.

2 | RESULTS AND DISCUSSION

2.1 | SEC-MALS analysis of ShuA–detergent complex in OPOE and DDM

Figure 1a shows the SEC profiles of ShuA in 1% OPOE at different protein concentrations ranging from 0.5 to 10 mg/mL injected onto a BioZen dSEC-2 column (5 mL) and monitored by UV absorbance at 280 nm. A single peak appears at $V_e \sim 2.8$ mL regardless of the amount of ShuA injected, with a very slight peak shift towards larger elution volumes as ShuA concentration increases. The extra protein-free micelles, which are not visible in the UV profile, are well separated from the ShuA–OPOE peak (see the refractive index profile in Figure S1). This good separation allows for the calculation of the PDC molar mass without contribution of protein-free micelle signals. The calculated molar mass of the ShuA–OPOE complex increases linearly as the injected concentration increases, from 150 to about 170 kDa (Figure 2a, Table S1). The small, regular, and linear increase in the "apparent" molar mass of the complex suggests attractive interactions between ShuA–OPOE complexes rather than uncertainties from light scattering (LS) measurements (the LS baselines are stable and the signal fluctuations are low) or oligomerization of the complex (the calculated mass throughout the peak is constant). A negative second virial coefficient (A_2), calculated from the Zimm equation (Equation 1) was found to be about -3.3×10^{-4} molmL/g^2, which is characteristic of attractive interactions between ShuA–OPOE complexes in 1% OPOE containing buffer. The molar mass of ShuA was calculated both with and without considering this second virial coefficient (Figure 2b). With an expected molar mass of ShuA of 70,860 Da from its His_6-tagged sequence, ShuA can be described as a monomer in OPOE, binding approximately 210–230 OPOE molecules. This is in agreement with the value of ShuA molar mass determined in OPOE by SEC-MALS just after the affinity column, prior to the concentration step (Figure S2, Table S2). The detergent-to-protein mass ratio (δ) was calculated at all concentrations (Figure 2c) and found to be ~0.9 g/g for ShuA–OPOE for the highest concentrations, showing that the ShuA–OPOE complex forms a stable complex suitable for further structural studies.

Figure 1b shows a distinct behavior for ShuA solubilized and purified in DDM and analyzed in 0.5 mM DDM. The UV elution profiles reveal a peak corresponding to the ShuA–DDM complex, which shifts significantly from $V_e \sim 2.9$ to ~2.5 mL as the ShuA concentration increases, with the peak at 3.3 mL corresponding to extra DDM micelles (also observed by refractometry, Figure S3a). In contrast to ShuA–OPOE, the calculated apparent molar mass of the ShuA–DDM complex increases asymptotically as the ShuA

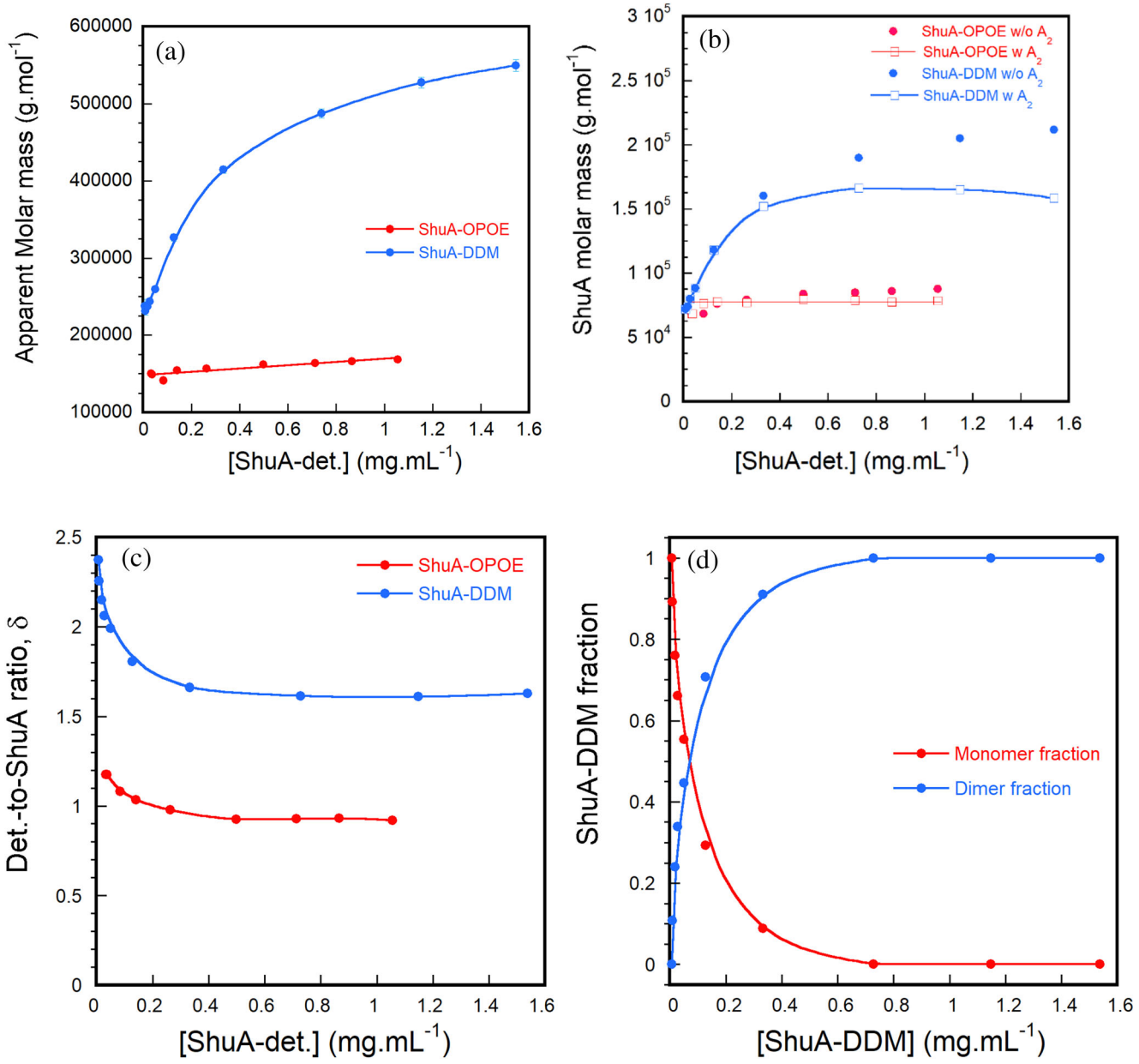

FIGURE 2 (a) Apparent molar masses of ShuA–detergent complex (○) (red for OPOE, blue for DDM). (b) Calculated molar mass of ShuA taking (●) or not taking (□) into account the second virial coefficient (red for OPOE, blue for DDM). (c) Bound detergent to ShuA ratio (δ) (red for OPOE, blue for DDM). (d) ShuA–DDM fraction into monomer and dimer form.

concentration rises from 240 to about 550 kDa (Figure 2a, Table S3a). Additionally, as the peak moves towards lower elution volumes (i.e., higher molar masses), the ShuA–DDM solution displays heterogeneous behavior throughout the peak (non-horizontal line) characteristic of variations in apparent molar mass. Finally, for the highest concentrations injected (>5 mg/mL), the SEC profiles overlap, while the complex's apparent molar mass continues to increase with the ShuA concentration (Figure S3b). As for OPOE, this suggests the presence of attractive interactions between oligomers of ShuA–DDM complexes. From the calculated mass fractions of ShuA and DDM (Table S3) and the mass ratio δ (Figure 2c), the complex at high concentrations appears structurally stable, with a constant DDM-to-ShuA ratio of ∼1.6 g/g. A second virial coefficient was determined from the high concentration range of the complex, that is, where the complex appears stable, and was found to be approximately -1.97×10^{-4} molmL/g^2. By accounting for these attractive interactions in the "*Protein Conjugate*" procedure (Equation 1), the molar mass of ShuA without interaction was calculated in 0.5 mM DDM (Figure 2b). The values ranging from about 71 to 165 kDa suggest that ShuA transitions from a monomer at low concentrations to a dimer at high concentrations.

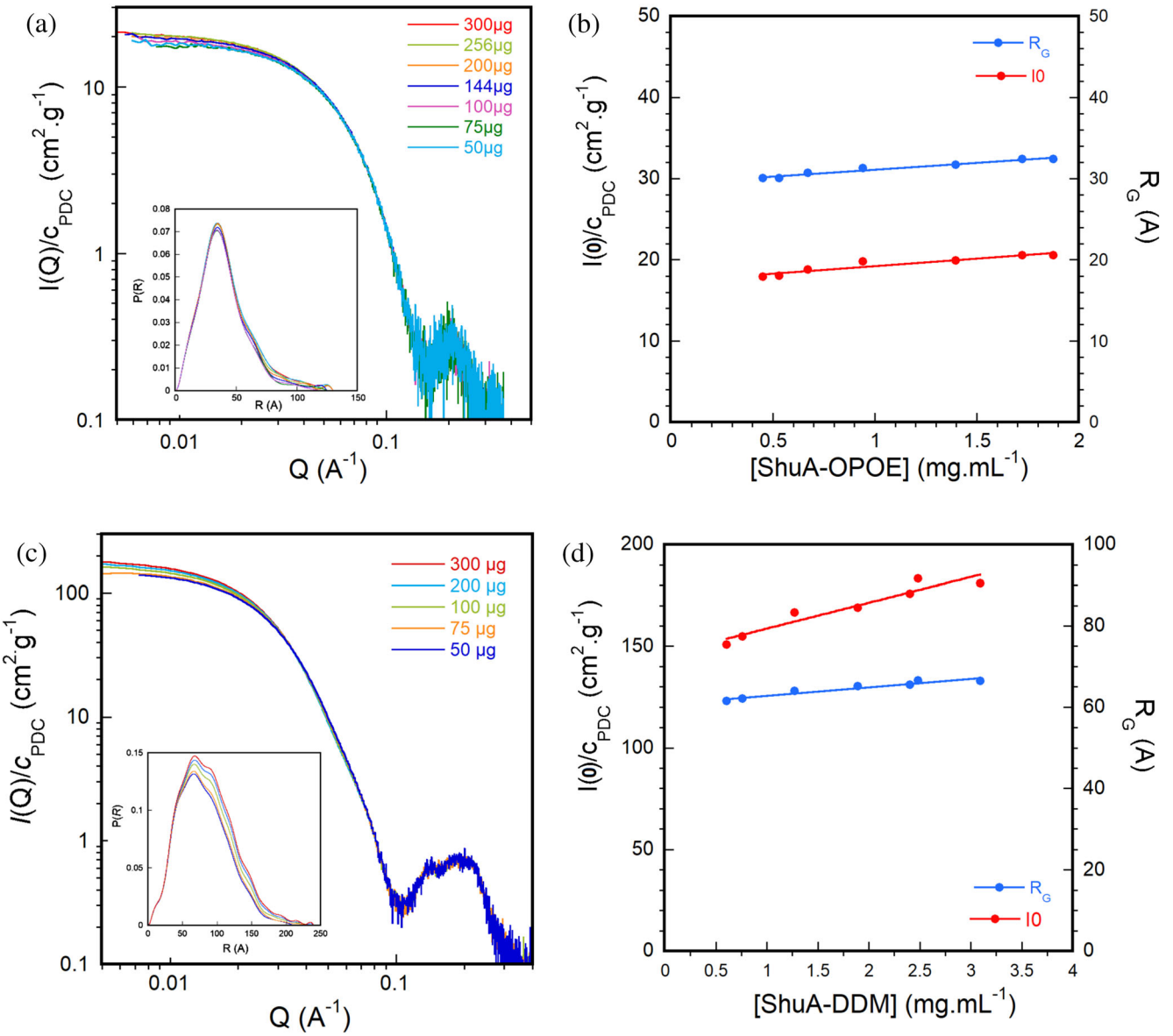

FIGURE 3 (a) Concentration-normalized scattering intensities of ShuA in OPOE at different injected amounts as a function of *Q*; PDDF plot in insert. (b) Forward intensity $I(0)/c_{PDC}$ and "apparent" radius of gyration R_G as a function of ShuA–OPOE complex concentration. (c) Concentration-normalized scattering intensities of ShuA in DDM at different concentrations as a function of *Q*; PDDF plot in insert. (d) $I(0)/c_{PDC}$ and "apparent" R_G as a function of ShuA–DDM complex concentration.

As a control, at low concentration just after the affinity column and prior to concentration, a SEC-MALS analysis confirms that ShuA in 0.5 mM DDM is monomeric, with approximately 300 molecules of DDM bound to the transmembrane domain (Figure S2, Table S2).

The monomer and dimer mass fractions were calculated (detailed equations in Appendix S2, Table S4) and plotted as a function of ShuA–DDM concentration taken at the maximum of the elution peak (Figure 2d). The inhomogeneity observed across the elution peak can therefore be interpreted as a monomer/dimer equilibrium that occurs during the elution. In order to thoroughly describe the structure and the behavior of the ShuA–detergent complex in 1% OPOE and 0.5 mM DDM, we performed SEC-SAXS experiments as a function of ShuA concentration.

2.2 | SEC-SAXS analysis of ShuA–detergent complex in OPOE and DDM

Two concentration-series of ShuA–detergent complex in 1% OPOE and 0.5 mM DDM between 1 and 15 mg/mL (i.e., between 50 and 300 µg injected on the BioZen column) have been measured by SEC-SAXS on the beamline SWING from synchrotron SOLEIL (St-Aubin, France). These concentrations correspond to the

TABLE 1 Structural parameters obtained from SEC-SAXS analysis.

Sample	R_G|D_{max} (Å/Å)
ShuA–1% OPOE (FF)	30.1|~95
ShuA–0.5 mM DDM (FF)	61.8|~208
ShuA–DDM (Abel et al., 2021)	42.2|~132
ShuA–0.5 mM moDDM/D_2O (exp. 10 mg/mL)	68.9|~230
ShuA–0.5 mM DDM/H_2O (exp. 15 mg/mL$^-$)	69.4|~235
ShuA–7.5 mM DDM (exp. 1 mg/mL)	48.7|~160

Note: Radius of gyration (R_G), maximum dimension (D_{max}) for ShuA–detergent complex in OPOE/H_2O, DDM/H_2O, and moDDM/D_2O (FF = form factor).

highest concentration range in the SEC-MALS experiments, where ShuA–detergent complex was found stable.

Figure 3a depicts the SAXS data analysis for ShuA in 1% OPOE. The absolute intensities have been normalized to ShuA–OPOE complex concentrations. All curves superimpose for $Q > 0.05$ Å^{-1}, whereas at low Q values, the intensity increases as the concentration of complex increases. The Guinier approximation in the low Q region allows one to determine both the forward intensity, $I(0)$, and an "apparent" radius of gyration, R_G, for all concentrations injected on the SEC column. The increase in $I(0)/c_{PDC}$ as a function of ShuA–OPOE concentration (Figure 3b) confirms the presence of attractive interactions between monodisperse complexes, as was observed by SEC-MALS. This is also confirmed by the increase in the "apparent" R_G with concentration and the pair distance distribution function (PDDF) plot (Figure 3a insert), whose bell shape is characteristic of a globular complex, and also by the Kratky representation (Figure S4b), which shows a compact complex without shape evolution. The variation in $P(R)$ for $R \sim D_{max}$ is likely due to attractive interactions. A second virial coefficient was calculated using Equation (11) and found equal to $\sim -3.5 \times 10^{-4}$ molmL/g^2 in agreement with the value from SEC-MALS. From the SAXS intensities, an "ideal" form factor (FF) was built by merging the low concentration curve (50 µg) at low Q to avoid weak interaction effects and the high concentration curve (300 µg) less noisy at high Q values. Structural parameters (R_G, D_{max}) of the ShuA–OPOE complex were determined (Table 1), which show a smaller complex in OPOE compared to the model previously described in DDM (Abel et al., 2021) and slightly larger than the atomic structure (3FHH.pdb). This is due to a low electron density contrast of the polyoxyethylene head group with solvent, as seen by SAXS, which reduces the X-ray scattering intensity of the micelle at low Q values (Figure S5a). The main contribution of the detergent signal in the ShuA–OPOE complex originates from the detergent tails, reducing the values of R_G and D_{max} of the whole complex.

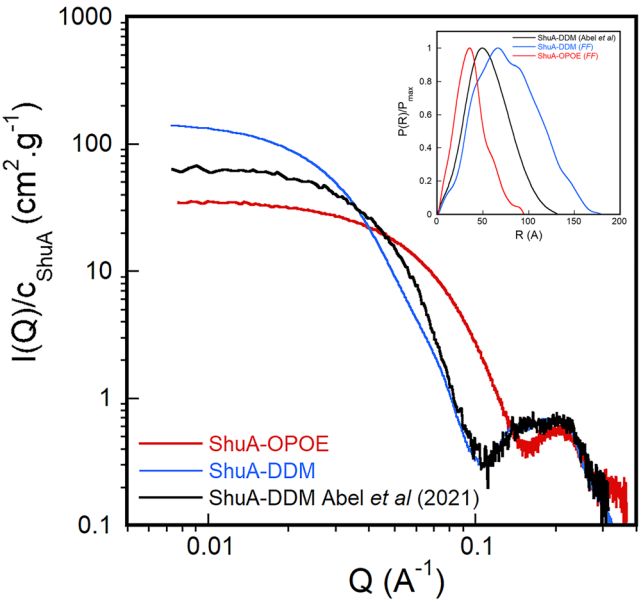

FIGURE 4 Experimental SAXS form factors of ShuA-OPOE (red line) and ShuA-DDM (blue line), obtained after merging low-ShuA concentration curve at small Q-values and high-ShuA concentration curve at large Q-values, compared to ShuA–DDM complex data from Abel et al. (2021) (black line).

Figure 3c shows the SAXS analysis for the ShuA–DDM complex. As for ShuA in OPOE, all SAXS curves superimpose at high Q-values between 50 and 300 µg injected into the column in agreement with SEC-MALS analysis and exhibit an increase in $I(0)/c_{PDC}$ and R_G as the concentration of ShuA increases (Figure 3d). However, the PDDF plot (Figure 3c insert) shows evolution in shape as a function of concentration with the appearance of a shoulder at ~100 Å from 100 µg injected ShuA–DDM that does not evolve as the concentration increases (Figure S4c). This shoulder could be the signature of dimers (Glatter & Kratky, 1982). This is consistent with the results from SEC-MALS that show an increase in molar mass, from monomer to dimer, up to 100 µg and then a stabilization in the ShuA–DDM dimer molar mass. As for SEC-MALS data analysis, a second virial coefficient was determined for concentrations between 50 and 300 µg injected and found $\sim -1.33 \times 10^{-4}$ molmL/g^2, slightly different from the one found with SEC-MALS ($\sim -1.97 \times 10^{-4}$ molmL/g^2) but still negative, suggesting attractive interactions between ShuA–DDM complex dimers. The dimensions of ShuA–DDM in this high range of concentration are larger (D_{max} between 210 and 240 Å) than those previously described (Abel et al., 2021). In this previous study, the concentration of the ShuA–DDM complex in the peak was between 0.03 and 0.06 mg/mL and the apparent molar mass of the complex between 220 and 235 kDa, which corresponds to the low concentration range in the present SEC-MALS study.

Regardless of the detergent used, ShuA–detergent complex appears as a globular assembly as evidenced by the double logarithmic plot, where $I(Q)$ is constant at small Q-values and decreases rapidly at intermediate Q-values, or the bell shape of both the PDDF and the Kratky plot. ShuA–OPOE forms a smaller complex than ShuA–DDM, as observed from the shift of the second maximum ($\sim 0.2\ \text{Å}^{-1}$) towards larger Q-values (Figure 4), and from the maximum dimension ($D_{max} \sim 95$ Å) in the PDDF plot (Figure 4 insert). In DDM, ShuA exhibits distinct behavior as compared to the previous study. While both curves superimpose at large Q-values, suggesting a common feature, the forward intensity for ShuA–DDM at higher concentrations increases, as well as R_G and D_{max}. This could be consistent with the formation of a dimeric complex, as observed by SEC-MALS at high concentrations.

In order to decipher the oligomeric state of ShuA at high concentrations and its spatial organization in DDM, we performed SANS in a matched-out DDM (moDDM), that is, a specifically deuterated DDM (in the head and tail regions) that is totally contrast matched in a 100% D_2O buffer solution (Midtgaard et al., 2018).

2.3 | SANS analysis of ShuA–moDDM complex

The SANS experiment was performed on the QUOKKA instrument[1] at ANSTO (Sydney, Australia) with ShuA initially prepared, that is, solubilized from outer membrane and purified with 1% OPOE, then exchanged with 1% DDM-H_2O on a concentrator device and finally exchanged with 0.5 mM moDDM/D_2O on a 24 mL-SEC column (S200 Increase 10/30). The fractions with maximum absorbance ([ShuA] = 0.8 mg/mL) were collected (Figure S7) and their SANS signal measured. The atomic structure of ShuA being available (3FHH.pdb), the theoretical scattering curve was calculated using CRYSON (Svergun et al., 1998) and compared to ShuA in moDDM/D_2O buffer (Figure 5). The monomeric structure of ShuA clearly does not coincide with the experimental SANS curve. To verify the results and the efficient exchange of detergent from OPOE to DDM and moDDM, the SANS experiment was reproduced on the D22 instrument[2] at ILL (Grenoble, France) with ShuA directly solubilized and purified using DDM and then exchanged with 0.5 mM moDDM in a 100% D_2O buffer on a 24 mL-S200 column as previously. The SANS signal of ShuA–moDDM at the highest concentration ([ShuA] = 0.83 mg/mL) is similar to the result from QUOKKA (Figure S8a). The expected $I(0)$ for a monomer of ShuA at 0.8 mg/mL is $\sim 0.047\ \text{cm}^{-1}$, whereas the experimental $I(0)$ for ShuA–moDDM in 100% D_2O buffer is found to be $\sim 0.235\ \text{cm}^{-1}$. The R_G of both curves, as well as the D_{max} from the PDDF (Figure 5, Table 2), suggest a large oligomer or a cluster of dimers (Valadez-Perez et al., 2021; Zhang et al., 2012) of ShuA in the matched-out DDM in D_2O, which could corroborate the SEC-MALS and SEC-SAXS results, where attractive interactions between dimers of ShuA–DDM complex were characterized. This cluster or large oligomer could be due to the effect of deuterated moDDM and/or D_2O that could induce stronger attraction between moDDM micelles (Figure S5b) compared to DDM micelles and therefore could increase attractions between ShuA–moDDM complexes.

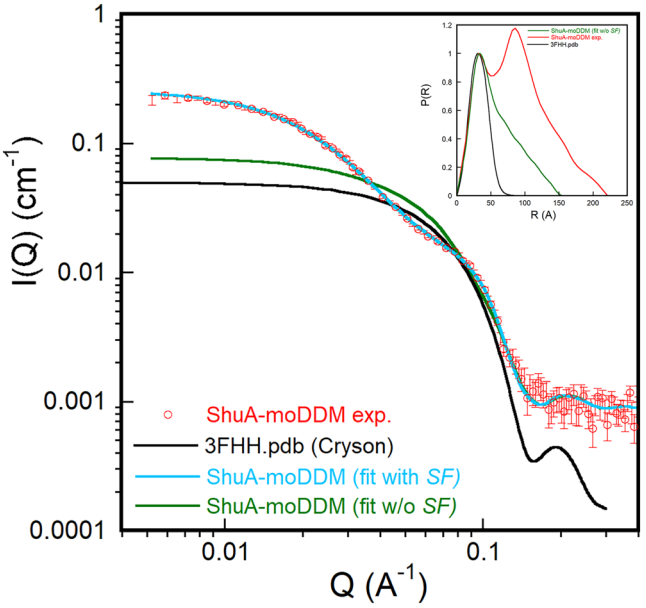

FIGURE 5 Experimental SANS curve of ShuA–moDDM (red dot) in 100% D_2O buffer (50 mM Tris, pD 7.5, 100 mM NaCl, 0.5 mM moDDM/D_2O). The curve is obtained by merging data from three sample-detector distances; SasView fitted curve of ShuA–moDDM (blue line) using a cylinder as form factor (FF) and a sticky hard-sphere structure factor (SF). The green curve represents the cylinder form factor alone. (Inset) Pair-distance distribution functions, $P(R)$, of ShuA 3FHH structure (black line).

To decipher the behavior of ShuA in moDDM and take into account attractive interactions, the SANS curve was fitted by using the program SasView (http://www.sasview.org/), as the product of a form factor $P(Q)$ and a structure factor $S(Q)$, which enables one to account for weak interactions. The theoretical SANS curve of ShuA 3D-structure was also fitted using SasView with either an ellipsoid model defined by its equatorial and polar radii (R_{eq}, R_{po}) or a cylinder model defined by its radius and length (R, L). By using the scattering length density calculator from BioISIS (http://psldc.isis.rl.ac.uk/Psldc/) with the ShuA sequence in 100% D_2O ($\rho_{ShuA} = 3.273 \times 10^{-6}\ \text{Å}^{-2}$ and $\rho_{buf} = 6.376 \times 10^{-6}\ \text{Å}^{-2}$), the best fit model for the

[1]During the long ILL shutdown.
[2]After the ILL shutdown.

TABLE 2 Structural parameters obtained from SANS analysis.

Sample	R_G (Å)|D_{max} (Å)|V_{Porod} (Å^3)	$I(0)$ (cm^{-1})	SasView model dimensions (Å|Å)
3FHH 0.8 mg/mL (Cryson)	24|∼76|∼94,600	0.047	R_{equ}. 26|R_{pol}. 39[a]
	24|∼76|∼94,600	0.047	R 25|H 57.4[b]
ShuA–moDDM (exp.)	66|∼220|∼350,000	0.235	
ShuA–moDDM (fit w/o SF)	46|∼155|∼176,000	0.142	R 23.6 | H 151[b]

Abbreviation: SF, structure factor.
[a]Ellipsoid model.
[b]Cylinder model.

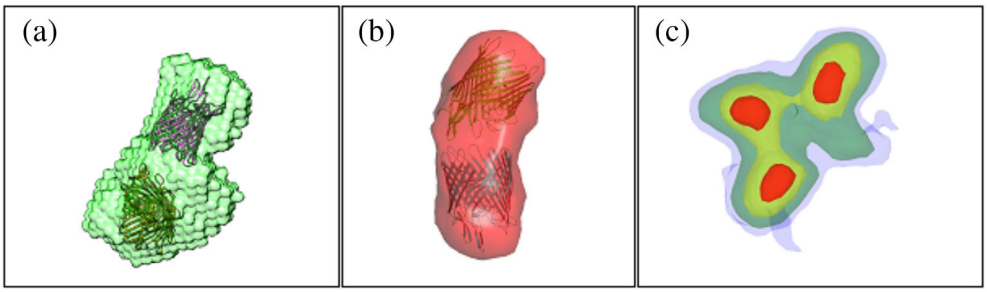

FIGURE 6 (a) Ab initio shape reconstruction from pair-distance distribution function of ShuA–moDDM using DAMMIF. (b) Electron density reconstruction from fitted scattering data of ShuA–moDDM using DENSS. In both cases, models were performed using the fitted curve without SF. The two ab initio models can be overlaid with two molecules of ShuA using PyMOL (Schrodinger LLC, 2015). (c) Electron density reconstruction from experimental SANS scattering data of ShuA–moDDM using DENSS (Snapshot from DENSS webserver interface). Electron densities are shown as volumes colored according to electron density.

3FHH-structure was a prolate ellipsoid ($\chi^2 = 11$) with $R_{eq} \sim 27$ Å and $R_{po} \sim 39$ Å (Figure S9a), which agrees well with the dimensions of ShuA measured using PyMOL (Schrodinger LLC, 2015) (i.e., β-barrel diameter ∼50 Å and β-barrel height ∼80 Å) (Figure S9c). The cylinder model was less good ($\chi^2 = 49$) with $R \sim 25$ Å and $L \sim 57.4$ Å (Figure S9b). For ShuA–moDDM in D_2O buffer, a cylinder model with a sticky hard-sphere (SHS) structure factor successfully accounts for the experimental SANS curve (Figure 5). The dimensions of the cylinder were found equal to ∼23.6 Å in radius and ∼151 Å in length, suggesting the formation of a linear dimer consisting of two ShuA monomers arranged end-to-end and stabilized by close intermolecular interaction. This is confirmed by the PDDF (Figure 5), which, in the small distance range, displays the characteristic feature of ShuA in its monomeric form. The PDDF of ShuA–moDDM, calculated without the contribution of $S(Q)$, displays the form factor of a ShuA dimer, with a maximum dimension and Porod volume approximately twice those of the ShuA monomer.

2.4 | Macromolecular modeling of ShuA in detergent from SAXS and SANS data

To gain valuable insights into the architecture and assembly of ShuA in detergent solutions, we combined two complementary strategies. First, we modeled SANS data using DAMMIF and DENSS to reconstruct the overall shape of ShuA in moDDM. Second, we applied SASbelt to SAXS data to visualize the detergent belt surrounding ShuA in OPOE and DDM. For the DAMMIF analysis, the overall shape of the ShuA–moDDM complex was reconstructed using the $P(R)$ function derived from the SasView fitting SANS curve, without including the SHS structure factor. The reconstruction was carried out through the Web server interface (https://www.embl-hamburg.de/biosaxs/atsas-online/) with 20 iterations completed and the resulting envelopes aligned and averaged using DAMAVER (Volkov & Svergun, 2003). For the DENSS analysis, 3D electron density maps were generated, either from the scattering intensity $I(Q)$ or the pair-distance distribution function $P(R)$ via the Web server (https://denss.ccr.buffalo.edu/). A total of 20 electron density maps were computed, aligned, and averaged to produce the 3D reconstructions. Both experimental SANS data and the SasView form factor were analyzed.

Figure 6a,b presents the ab initio models obtained for the SasView FF from SANS using DAMMIF and DENSS, respectively. Each suggests that ShuA in 0.5 mM moDDM forms a rather linear dimeric structure with close interactions. Additionally, a DENSS reconstruction of the experimental SANS curve suggests that the solution at very low Q-values may consist of a cluster of three ShuA assemblies (Figure 6c). This aligns with forward intensity values suggesting a hexamer or a cluster of three dimers. This behavior, which was not

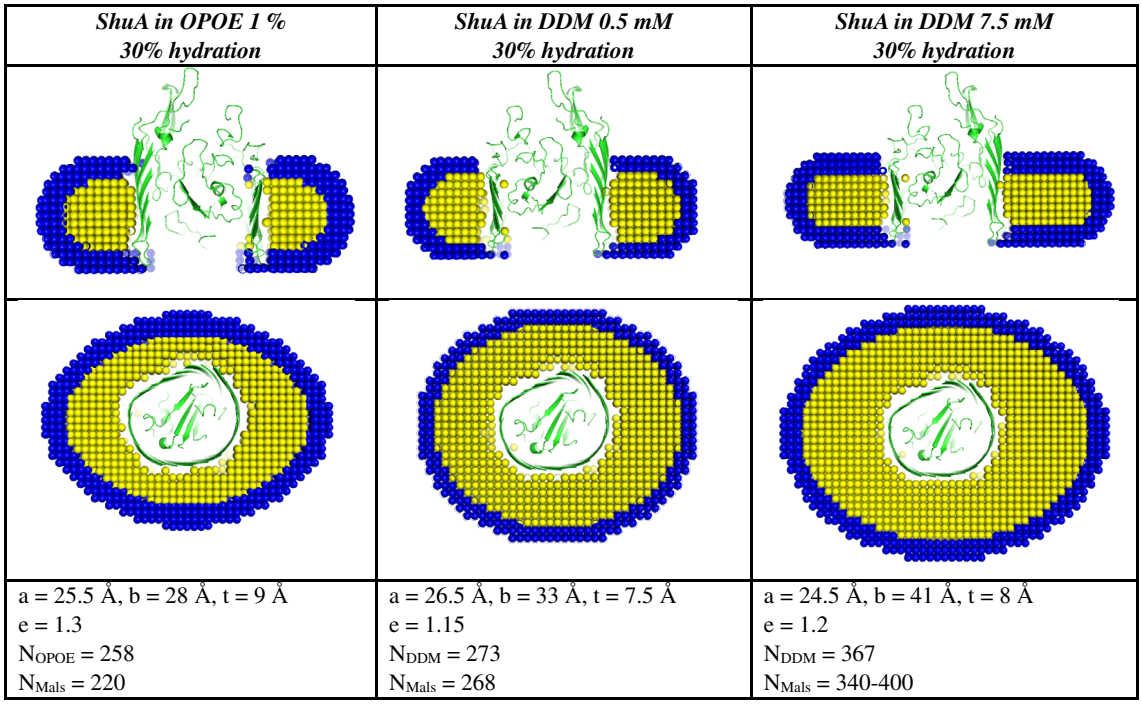

FIGURE 7 SASbelt-derived models of the detergent belt surrounding ShuA in 1% OPOE and in 0.5 and 7.5 mM DDM. Side- and top-views are shown, with blue beads highlighting the hydrophilic region and yellow beads for the hydrophobic region of the belt. Geometric parameters for each model are indicated, and detailed input values plus fit results are provided in the SI. N_{OPOE} and N_{MALS} correspond to the number of detergent molecules *per* belt as determined by SASbelt modeling and by MALS, respectively.

observed in SAXS data with the protiated ShuA–DDM complex in H_2O buffer, could originate from the presence of moDDM in D_2O.

Figure 7 displays the ellipsoidal core–shell torus models generated by SASbelt, where blue and yellow beads represent the hydrophilic and hydrophobic regions of the detergent belt, respectively. As expected, the belt dimensions are smaller in OPOE than in DDM, consistent with a reduced PDC in the OPOE condition. The slightly greater ellipticity of the ShuA/OPOE model ($e = 1.3$), as shown in Figures 7 and S13a, may indicate increased shape variability or structural disorder in the OPOE belt compared to the more uniform DDM cases ($e = 1.15$ and 1.2 for 0.5 and 7.5 mM DDM, respectively).

Using 30% hydration for the detergent heads yielded excellent fits (Figure S13) with $\chi^2 = 0.7$ for 0.5 mM DDM, $\chi^2 = 1.8$ for 1% OPOE, and a poorer but acceptable fit ($\chi^2 = 10.7$) at 7.5 mM DDM. The head-to-tail ratios—ideally unity—were 1.14 (0.5 mM DDM), 1.01 (1% OPOE), and 0.90 (7.5 mM DDM). The aggregation numbers in OPOE and DDM from SASbelt agree well with those from SEC-MALS, confirming the reliability of the modeling.

2.5 | SAXS comparison of ShuA–DDM/H_2O and ShuA–moDDM/D_2O complexes

Samples prepared for SANS experiments typically require deuterated compounds such as (per)deuterated proteins or (per)deuterated detergents, in H_2O/D_2O solvent mixtures. In this study, ShuA was prepared using moDDM in 100% D_2O buffer, allowing us to focus on characterizing the protein structure while matching out the contribution from the detergent. To evaluate the influence of moDDM and D_2O on the structure of the ShuA–DDM complex in solution, we compared by SAXS, ShuA–moDDM in 100% D_2O buffer with ShuA–DDM in H_2O buffer. The ShuA–moDDM/D_2O sample preparation for SAXS was identical to that for the SANS experiment: ShuA–DDM was injected onto a 24 mL-S200 column pre-equilibrated with a deuterated moDDM-containing D_2O buffer solution. The UV-elution profile of ShuA–moDDM/D_2O was compared to the elution profiles on the same column of a concentrated ShuA–DDM/H_2O sample (15 mg/mL) and a diluted ShuA–DDM sample after the affinity column (Figure S10). Both concentrated ShuA–DDM (15 mg/mL) and ShuA–moDDM (10 mg/mL) eluted at $V_e \sim 9$ mL whereas the monomeric ShuA eluted at $V_e \sim 11$ mL confirming the dimerization of ShuA at high concentrations. The concentrated ShuA–DDM sample (15 mg/mL) was analyzed by SEC-SAXS on SWING at SOLEIL, whereas all fractions through the peak of ShuA–moDDM were collected and analyzed by SAXS in batch mode on the BM29 beamline at ESRF. For each fraction, $I(0)$, R_G, and D_{max} were determined (Table S6). Fractions 15–19, which exhibited similar shapes and values of R_G, were averaged for further

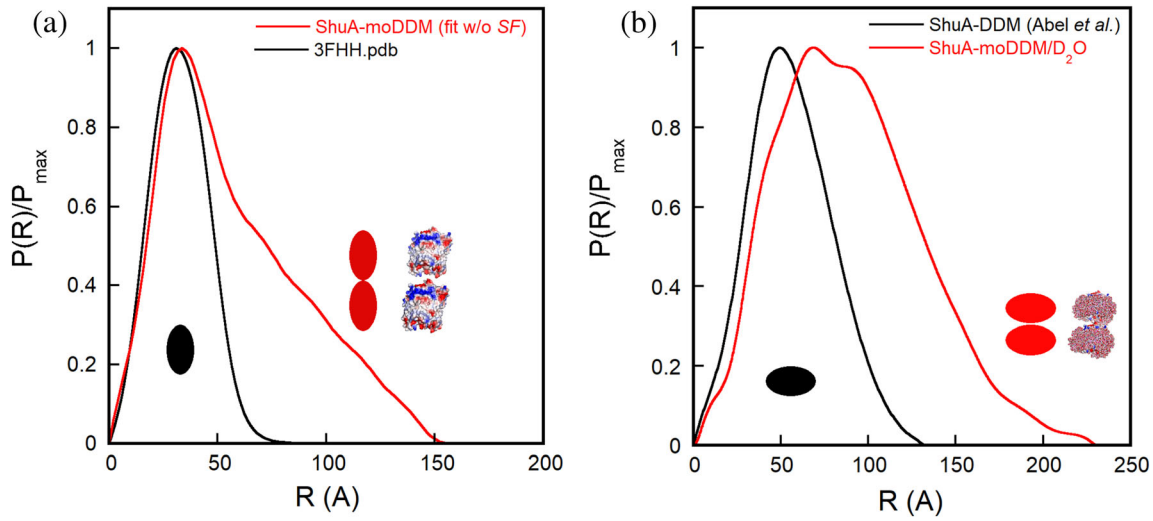

FIGURE 8 (a) Representative view of ShuA as linear dimer as suggested by the SANS PDDF. (b) Representative view of ShuA–DDM complex as parallel dimer as suggested by the SAXS PDDF.

analysis. The scattering curves $I(Q)/c_{ShuA}$ and $P(R)/P_{max}$ for both ShuA–DDM/H_2O buffer and ShuA–moDDM/D_2O buffer at the maximum absorbance show similar shapes and dimensions (R_G, D_{max}) (Figure S8b, Table 1), indicating that the presence of the deuterated detergent and the use of D_2O in the buffer neither affect the detergent belt surrounding ShuA nor the oligomeric state of the protein. However, the strength of the attractive interactions between dimers of ShuA–moDDM complexes could not be evaluated as this would have required injecting a series of more concentrated samples onto the column, which could not be achieved.

2.6 | SAXS/SANS comparison of ShuA–moDDM for dimer organization

Analysis of SEC-MALS, SEC-SAXS, and SANS experiments as a function of ShuA concentration suggests that the ShuA–DDM complex in a buffer containing 100 mM NaCl, 0.5 mM DDM at pH 7.5 forms a dimer at concentrations above 5 mg/mL (concentration measured prior to injection onto SEC column). However, the precise arrangement of this dimer—whether side-by-side, end-to-end, or an intermediate form, and whether involving weak or strong interactions—remains unclear. By comparing the PDDFs of ShuA–moDDM from SAXS and SANS experiments, we propose a dimer arrangement for ShuA and its complex in DDM. Based on the values of maximum dimension and Porod volume (Tables 1 and 2) as well as the shape of the PDDFs (Figure 8a) for the 3FHH structure of ShuA and the fitted SANS curve of ShuA–moDMM without the SHS structure factor, we observe that both D_{max} and V_{Porod} double. Moreover, the $P(R)$ of ShuA–moDDM dimer closely superimposes with that of the ShuA monomer for $R < 50$ Å, and then decreases linearly up to twice the D_{max} of ShuA monomer, suggesting a linear arrangement, along the polar axis, of two prolate ellipsoids (Glatter & Kratky, 1982). In contrast, comparing the PDDFs of ShuA–DDM complexes at low and high concentrations (Figure 8b), D_{max} does not double for concentrated ShuA, and a shoulder appears that could be consistent with two prolate ellipsoids, superimposed along their equatorial axes (Glatter & Kratky, 1982). Both results from SANS and SAXS are consistent with an end-to-end ShuA dimer when regarding the complex with the matched-out belt and with two superimposed monomers of ShuA–DDM complex when regarding the whole complex (schematic models inserted in Figure 8). ShuA in 0.5 mM DDM therefore seems to form a colloidal dimer of ShuA–DDM complexes rather than a side-by-side dimer of ShuA embedded in a DDM belt. This is consistent with the fact that the majority of known 3D structures of 22-stranded transmembrane β-barrels are monomeric (Tamm et al., 2004).

2.7 | Colloidal behavior of ShuA in detergent solution

The present study of ShuA in OPOE and DDM using SEC-MALS and SAS techniques reveals two distinct behaviors regarding the oligomerization of the ShuA–detergent complex. In 1% OPOE (~4×CMC), the ShuA–detergent complex remains monomeric, exhibiting inter-complex attractive interactions that induce an increase in the apparent molar mass of the complex. However, this does not lead to the formation of PDC dimers. In contrast, in 0.5 mM DDM (~3×CMC), the ShuA–DDM complex in solution evolves into a

reversible monomer/dimer equilibrium as a function of ShuA concentration, with ShuA–DDM dimers displaying attractive interactions at the highest ShuA concentrations.

To assess whether the observed behaviors are influenced by the nature or by the concentration of detergent in the ShuA solution, SEC-MALS experiments were conducted by modifying the composition of the ShuA–DDM solution. Ionic strength, pH, and DDM concentration were tested individually. Changing the NaCl concentration from 100 to 300 mM, or lowering the pH from 7.5 to 5.0 (close to ShuA's pI) did not significantly affect the behavior of the ShuA–DDM complex with 0.5 mM DDM (i.e., complex dimer formation) (Figure S11a). Modulating the ionic strength with NaCl or reducing the net charge of ShuA increased the apparent molar mass, likely due to stronger attractions between dimers. In contrast, increasing the DDM concentration in the mobile phase from 0.5 to 7.5 mM seemed to prevent dimer formation. A linear increase in apparent molar mass of the ShuA–DDM complex as the injected concentration of sample increases, similar to that observed with 1% OPOE, suggested attractive interactions between ShuA–DDM monomeric complexes. A similar trend was observed for the DDM-to-ShuA ratio (δ), which was not significantly affected by changes in NaCl concentration or pH, but increased with higher DDM concentrations (Figure S11b) and gradually decreased as the ShuA–DDM complex concentration increased. The increase in the DDM-to-ShuA ratio, indicating a larger detergent belt with increasing DDM concentration, as observed with the SASbelt modeling, has already been described in other studies (Kaufmann et al., 2006; Wolfe et al., 2019) and also modeled by MD simulations in our previous study (Abel et al., 2021). This can be explained by the tendency of DDM to energetically favor adsorption onto the protein surface rather than formation of micelles in the bulk (Polidori et al., 2016), whereas the leakage of the detergent from the belt to the bulk could result from the increase in attractive interactions between ShuA–DDM complexes (Gelbart et al., 1984).

To understand the mechanisms controlling ShuA–detergent behavior in the two detergents, we therefore analyze the composition of the ShuA solution in each detergent. For OPOE, the detergent concentration used in the mobile phase for purification, SEC-MALS, and SAS experiments was 1% (~28.6 mM). With a *CMC* of 6.6 mM and an aggregation number of approximately 120% ± 10% molecules per micelle (from our SEC-MALS experiments), the molar concentration of OPOE micelles is ~170 μM. In our study, ShuA concentrations injected onto the SEC column ranged from 1 to 10 mg/mL, resulting at the maximum of the elution peak in ShuA–OPOE complex molar concentrations between 2 and 8 μM, which is much lower than the OPOE micelle molar concentration.

For DDM, the concentration used in all SEC experiments was 0.5 mM, which corresponds (with $N_{ag} \sim 135$ molecules per micelle and CMC ~ 0.17 mM) to ~2.3 μM of DDM micelles, which is almost 100 times less than OPOE. The molar concentrations of ShuA–DDM dimers in the elution peak ranged from 0.9 to 4.2 μM, which is roughly the same order of magnitude as the DDM micelle concentration. In contrast, the molar concentrations of ShuA–DDM monomer complexes ranged from 0.02 to 0.08 μM, which is much lower than the DDM micelle molarity. These results are in line with the works of (Fleming (2002)), which show that when the protein is diluted in a detergent micelle phase, it moves towards a dissociated state. Thus, in 1% OPOE, the detergent micelle concentration being greater than the PDC concentration, the ShuA–detergent complex remains in a monomeric form. This behavior is further confirmed by SEC-MALS and SEC-SAXS experiments conducted with a higher concentration of 7.5 mM DDM in the elution mobile phase. Figure 9 shows the calculated molar mass for the ShuA complex, the protein alone, and the protein-bound detergent at 0.5 and 7.5 mM DDM from SEC-MALS analysis. At 7.5 mM DDM, the apparent molar mass of the ShuA–DDM complex increases linearly with ShuA concentration, similar to observations made for ShuA in 1% OPOE, suggesting a comparable behavior. A second virial coefficient, calculated from MALS data ($A_2 \sim -3.3 \times 10^{-4}$ molmL/g^2) indicates attractive interactions between ShuA–DDM complexes. The corrected molar mass of the ShuA–DDM complex (Table S3b), derived from A_2, suggests a monomer binding approximately 340–400 DDM molecules at 7.5 mM DDM, with the number of bound DDM molecules decreasing as ShuA concentration increases. This behavior is confirmed by the SAXS experiments. A concentration series between 1 and 6 mg/mL (i.e., between 75 and 300 μg injected on the BioZen column) was measured by SEC-SAXS on SWING (SOLEIL). The complex concentration-normalized intensities (Figure S12) show an increase in $I(0)/c$ and a decrease in the second maximum as ShuA concentration increases. The decrease in the second maximum ($Q \sim 0.2$ Å^{-1}) correlates with a release of DDM molecules from the protein belt to the detergent bulk solution as observed in SEC-MALS experiment (Figure S11b) and already reported (Abel et al., 2021), whereas the increase in $I(0)/c$ can be attributed to the attractions between ShuA–DDM complexes. This attraction between complexes could originate from the presence of the large amount of extra detergent micelles in the bulk solution (Jia et al., 2005). Indeed, in the latter experiment with 7.5 mM DDM, the molar concentration of DDM micelles (~54 μM) is larger than the ShuA–DDM molarity, which ranged from 0.3 to 7.9 μM in the elution peak.

The observed outcomes can be understood by considering the complex interplay of inter-particle

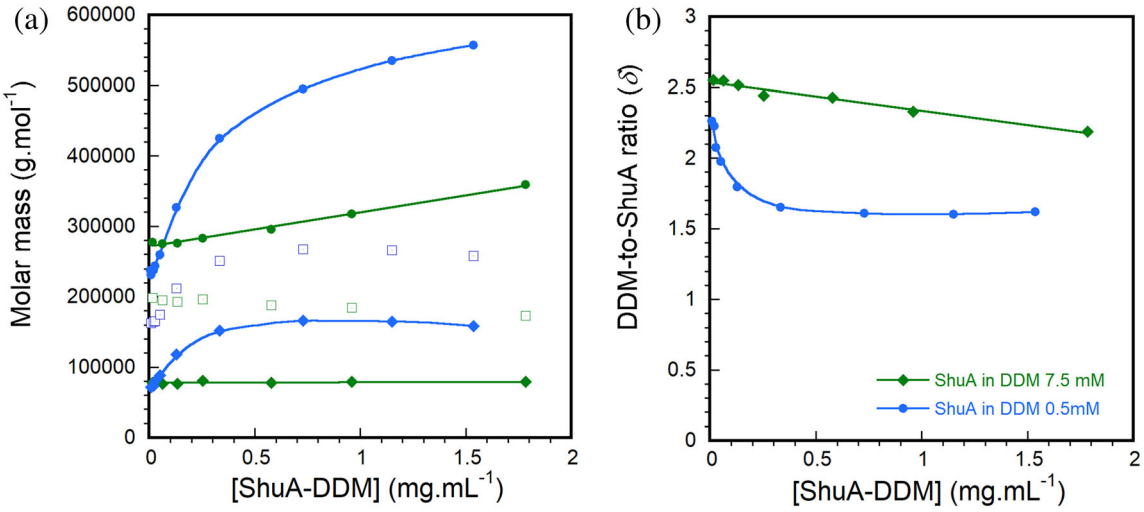

FIGURE 9 (a) Apparent molar masses of ShuA–detergent complex (●) calculated from SEC-MALS experiments with different detergent concentrations in the mobile phase (blue for 0.5 mM DDM, green for 7.5 mM DDM); calculated molar mass for ShuA (◆) and bound DDM (▫) by taking A_2 into account. (b) Bound detergent to ShuA ratio (δ) (blue for 0.5 mM DDM, green for 7.5 mM DDM).

interactions within the solution. In PDC solutions, several types of interactions are at work: those between detergent micelles, between PDCs, and between protein-free micelles and PDCs. These include both attractive forces—such as van der Waals interactions, hydrophobic interactions, and depletion interactions—and repulsive forces, including excluded volume effects, electrostatic repulsion, and hydration forces. While proteins experience repulsion due to excluded volume, net charge, and hydration shells, the repulsive interactions between micelles can paradoxically lead to attractive forces between PDCs, like the polymer-induced depletion attractions seen in colloid or macromolecular systems (Asakura & Oosawa, 1958; Marenduzzo et al., 2006).

If it is relatively straightforward to study and characterize weak interactions between soluble proteins in salts, PEGs, or detergents (Bonneté et al., 1999; Jia et al., 2005; Kulkarni et al., 2000), characterizing the interactions between PDCs in solution is more challenging due to the presence of micelles. This can be overcome by using SAS techniques coupled in-line with SEC, which permits the separation of protein–detergent complexes from extra detergent micelles and the subtraction of surrounding micelle signal. It is also possible to assess the nature of inter-complex interactions for integral MPs (IMPs) like ShuA by looking at the interactions between protein-free micelles. Indeed, in 2000's, Hitscherich and co-workers have shown that for IMPs embedded in a detergent belt, the interactive behavior of IMP–detergent complexes follows that of protein-free detergent micelles, suggesting that the detergent contribution dominates in the behavior of the PDC (Hitscherich et al., 2000).

In our study, we characterized by SAXS the size, shape, and inter-micelle interactions of DDM, OPOE, and moDDM in solution (Figure S5). As previously described (Barret et al., 2013), the DDM micelle is stable in shape and presents an oblate core–shell ellipsoid structure, with R_G of ~32 Å and D_{max} of ~80 Å, exhibiting slight repulsive interactions as seen by the decrease in concentration-normalized forward intensity as the detergent concentration increases. For polyoxyethylene amphiphiles, to our knowledge, there are few studies addressing their micelle structure (Lang & Glatter, 1996; Zulauf et al., 1985). Our SAXS experiments do not allow for a clear characterization of OPOE micelle interactions at small Q-values; however, we could model the OPOE micelle at 1% using SasView. A spherical core–shell model allows us to fit the SAXS data (Figure S6), yielding a hydrophobic radius of ~9.3 Å, which agrees rather well with the C8-alkyl chain length using Tanford's formula (Tanford, 1980), and a shell thickness of ~23.3 Å. The shape of the scattering curve $I(Q)$ at low Q-values and the shell scattering length density from SasView fit ($Sld_{shell} \approx Sld_{water}$) suggest that the OPOE micelles are strongly hydrated, which could induce repulsive inter-micellar interactions. For moDDM in D_2O, the micelles can be modeled by an oblate core–shell ellipsoid structure with a radius of gyration $R_G \sim 36$ Å and a maximum dimension $D_{max} \sim 85$ Å, exhibiting strong attractive interactions as seen by the increase in concentration-normalized forward intensity as the detergent concentration increases (Figure S5b) and the value of $A_2 \sim -8.7 \times 10^{-4}$ molmL/g^2 (Table S7), the form factor remaining constant for $Q > 0.7$ Å^{-1}. Although DDM and moDDM micelles have similar shapes and dimensions (Table S7), the presence of the deuterated chain in moDDM enhances hydrophobic interactions between chains inside the micelles, thereby increasing overall inter-micelle interactions.

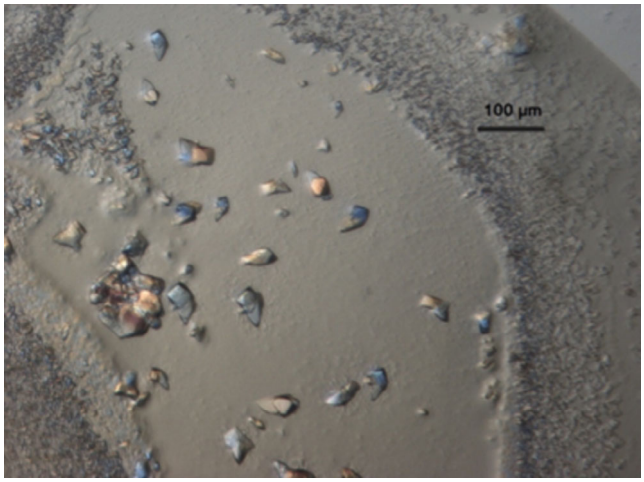

FIGURE 10 Crystallization trial of ShuA in 0.5 mM DDM at a concentration where it forms a colloidal dimer. The crystallization was done using the vapor-diffusion technique (reservoir solution: 35% PEG 300, 100 mM NaCl, 100 mM Na-citrate pH 5; hanging droplet: 1 µL ShuA at 5 mg/mL in 50 mM Tris pH 7.5, 150 mM NaCl, 0.5 mM DDM + 1 µL reservoir).

Additionally, D_2O can influence these inter-micelle interactions by altering the hydration shell—owing to the stronger deuterium bonding—further affecting the interactions between ShuA–moDDM complexes in a D_2O buffer (Reslan & Kayser, 2018). The presence of deuterated chains, if it neither alters the detergent belt around ShuA nor affects the dimer shape (Figure S8) induces a strong attraction (SHS) between dimers as seen in the SANS experiment fitting model. These deuteration effects observed with a ShuA clustering at small *Q*-values could possibly explain the results on SERCA or LamB in the paper of Midtgaard et al. (2018), where a combination of different oligomers and a minor fraction of aggregates were necessary to fit experimental data.

To explain the behavior of ShuA in detergent, one has to consider the protein embedded in its detergent belt and the effect of protein-free extra micelles. For low detergent micelle concentrations such as 0.5 mM DDM, the detergent adsorbs on the hydrophobic transmembrane domain of ShuA, favoring repulsions between complexes while keeping enough charged patches of the extra cellular surfaces accessible for van der Waals attractions. When ShuA concentration increases, attractions can occur between charged patches of ShuA, leading to end-to-end alignment of ShuA into dimers. When DDM in H_2O buffer is replaced with moDDM in D_2O buffer, the combination of the deuterated DDM belt and the presence of D_2O strengthens the attractive forces between dimers, leading to clustering of ShuA–moDDM dimers (Figure 6c). In contrast, for high concentrations of detergents, for example, 1% OPOE or 7.5 mM DDM, ShuA is embedded in a strongly hydrated belt or a larger detergent belt, which prevents attraction between charged patches of the protein and keeps the complex in a monomeric state, while the large amount of protein-free detergent micelles induces a depletion attraction between ShuA–detergent complex monomers (Jia et al., 2005).

These results demonstrate the critical influence of detergent type and concentration on the colloidal stability and oligomeric state of MPs in solution. The contrasting behaviors of ShuA in OPOE and DDM highlight the importance of optimizing detergent conditions to maintain monodispersity (monomer or dimer) and structural integrity, particularly for structural studies such as X-ray crystallography and cryo-EM. A key finding is that the oligomeric state of ShuA is not solely dictated by detergent type but also by the protein-to-detergent ratio. While ShuA remains monomeric in OPOE (and in Octyl Glucoside (OG), data not shown), it exhibits a concentration-dependent monomer/dimer equilibrium in DDM. This suggests that free detergent micelle content can modulate protein–protein interactions in a manner similar to polymer in protein crystallization, a factor often overlooked in structural studies and which can influence crystallization mechanisms. Surprisingly, the formation of dimers did not prevent the crystallization of ShuA at 5 mg/mL in 0.5 mM DDM-containing buffer, induced by the depletion attraction of PEG present as a crystallizing agent, as seen in Figure 10. Improvements in the crystallization of ShuA in DDM are still in progress in order to decrease the supersaturation and improve the crystal size and then determine if a dimer exists in the asymmetric unit or if it only acts as a precursor of crystallization.

Finally, by integrating SEC-MALS, SAXS, and SANS, our study provides a robust framework for characterizing protein–detergent interactions. These findings emphasize the need for a quantitative approach to detergent selection, ensuring that membrane protein samples are optimally prepared for structural and functional investigations.

3 | CONCLUSIONS

In this study, we explored the influence of OPOE and DDM on the colloidal behavior of the ShuA–detergent complex in solution. By combining SEC-MALS, SAXS, and SANS techniques, we revealed significant differences in the oligomeric state of the complex depending on the type and concentration of detergent. Our findings demonstrate that the ShuA complex remains monomeric in the presence of OPOE, with weak attractive interactions between PDCs. In contrast, in DDM, ShuA exhibits a reversible monomer/dimer equilibrium, influenced by protein concentration and protein-free detergent micelle concentration in solution. Increasing the DDM concentration tends to stabilize the monomeric form, highlighting the critical role of the protein-to-detergent ratio in complex structuring.

These results have direct implications for membrane protein crystallization. Since successful crystallization requires monodisperse and stable protein samples, our study underscores the necessity of optimizing detergent selection and concentration to prevent unwanted oligomerization or aggregation. Furthermore, the weak attractive interactions between PDCs, as observed in our experiments, suggest that detergent micelles can modulate protein–protein interactions, potentially influencing the nucleation mechanism and crystal packing. Additionally, our findings highlight the importance of distinguishing true physiological oligomeric states from detergent-induced associations, as misinterpretations could lead to inaccurate structural models. Ultimately, by carefully controlling detergent conditions, future studies can enhance the success rate of membrane protein crystallization and improve the accuracy of structural interpretations.

4 | MATERIALS AND METHODS

4.1 | Detergents and protein solutions

All salt and buffer reagents were purchased from Sigma. Octyl polyoxyethylene (OPOE) was purchased from Bachem (Octyl-POE, formula $CH_3(CH_2)_6CH_2(OCH_2CH_2)_nOH$, CAS number 27252-75-1; CMC (critical micelle concentration) ≈ 6.6 mM/0.23%; MW ≈ 350 g/moL (Rosenbusch et al., 2001)) and *n*-dodecyl-β-D-maltoside (DDM) from Anatrace (CAS number 69227-93-6; CMC ≈ 0.17 mM/0.0087%; MW ≈ 510.6 g/moL). The match-out DDM (moDDM, formula $C_{24}H_{15.8}D_{30.2}O_{11}$; MW ≈ 540.87 g/moL) used for SANS experiments on DDM-solubilized MPs (Midtgaard et al., 2018) was synthesized at the National Deuteration Facility (NDF-ANSTO, Sydney) as described in Appendices S1 and S2.

The recombinant ShuA was prepared either in OPOE or DDM-containing buffers for SEC-MALS and SAS experiments, as described below.

4.2 | ShuA preparation

The ShuA plasmid was a kind gift of Dr. K Brillet (Strasbourg). Expression, solubilization, and purification in OPOE were done on the basis of Brillet et al. (2009) with some improvements to reduce the number of steps. A new protocol was established with solubilization and purification in DDM.

4.2.1 | ShuA overexpression and crude bacterial membrane fraction preparation

To increase the amount of ShuA targeted to the outer membrane, overexpression was performed using the strain *E. coli* BL21 (DE3) Gold ΔABCF, in which the genes encoding the most abundant porins (OmpA, OmpC, OmpF, and LamB) have been deleted (Meuskens et al., 2017). Bacteria transformed with the pET20b-ShuA plasmid were grown at 30°C in Difco LB Lennox broth supplemented with 0.1 mg/mL ampicillin. When the OD_{600} reached about 0.5, induction was started with 1 mM isopropyl-D-1-thio-galactopyranoside (IPTG) for 3 h at 30°C. At the end of induction (OD_{600} around 0.8), bacteria were harvested by centrifugation at 3500*g* and resuspended in 0.5 M sucrose, 50 mM Tris HCl pH 8 buffer at a ratio of 4.5 mL/L culture. After resuspension of the bacteria, 1 mg/mL lysozyme and 2.5 U/mL Benzonase were added for 20 min at 4°C under magnetic stirring. An equal volume of 50 mM Tris–HCl pH 8 and 1.5 mM EDTA was then added and kept under magnetic stirring for 20 min at 4°C. At the end of this step, the spheroplasts were harvested by centrifugation at 3500*g* for 45 min at 4°C. The spheroplasts were resuspended in 0.2 M sucrose, 50 mM Tris–HCl pH 8, 2.5 U/mL Benzonase, 1% (v/v) PMSF, and 1% (v/v) Halt™ protease inhibitor cocktail. Lysis was performed by two passages through a French press (20,000 psi) and the unbroken material was removed by centrifugation (45 min at 3500*g*, 4°C). The crude membranes were harvested by ultracentrifugation (100,000 *g* for 90 min at 4°C) and resuspended in 50 mM Tris–HCl pH 8, 1 mM EDTA. Finally, a second ultracentrifugation was performed; the crude membrane fraction was resuspended at approximately 20 mg/mL and the material was stored at −80°C after freezing in liquid nitrogen.

4.2.2 | Solubilization and purification of ShuA in OPOE

The crude bacterial membrane fraction was solubilized at 5 mg/mL in 50 mM Tris–HCl pH 8, 1 mM EDTA, 1% (w/v) N-lauroyl-sarcosine for 60 min at 25°C. Then, an ultracentrifugation at 100,000 *g* for 60 min was performed and the sedimented fraction was solubilized for 60 min at 25°C in 50 mM Tris–HCl pH 8, 150 mM NaCl, 20 mM imidazole, 0.1 mM EDTA, 1% (v/v) OPOE. After a last ultracentrifugation at 100,000 *g* for 60 min at 25°C, the supernatant fraction was used for a one-step purification on a Ni-NTA column (from Cytiva). The eluate fraction was dialyzed against 50 mM Tris–HCl pH 8, 150 mM NaCl, 1% (v/v) OPOE to remove imidazole and concentrated to 10 mg/mL by ultrafiltration using 100 kDa MWCO Vivaspin 6 concentrators and frozen at −80°C for further experiments.

4.2.3 | Exchange of OPOE for DDM

ShuA at 10 mg/mL in 1% OPOE was diluted to 0.2 mg/mL in 50 mM Tris HCl pH 7.5, 1% (w/v) DDM. The

solution was then concentrated using a 100 kDa MWCO Vivaspin 6 to a volume of 0.1 mL. This step was repeated three times. After exchange, the ShuA–DDM complex was frozen at −80°C at 10 mg/mL.

4.2.4 | Solubilization and purification of ShuA in DDM

The same protocol as for OPOE was used with minor modifications. The solubilization with DDM was carried out in 50 mM Tris–HCl pH 8, 150 mM NaCl, 20 mM imidazole, 0.1 mM EDTA, 1.2% (w/v) DDM for 2 h at 25°C. The purification step on Ni-NTA was performed after a 12-fold dilution in 50 mM Tris–HCl pH 8, 150 mM NaCl, 20 mM imidazole to obtain a final concentration of 0.1% DDM. This step was necessary for the binding of ShuA to the Ni-NTA resin. Finally, the eluted fractions were dialyzed against 20 mM Tris–HCl, pH 8, 100 mM NaCl, 1 mM EDTA, 0.5 mM DDM and concentrated at 10 mg/mL for further experiments.

4.3 | SEC-MALS experiments on ShuA–detergent complexes

SEC-MALS (i.e., size exclusion chromatography coupled to multi-angle light scattering) experiments were carried out on a Shimadzu HPLC-UV system coupled to an Optilab™ T-rEX refractometer and a miniDawn™ TREOS MALS detector (Wyatt Technology). Two types of SEC columns connected to a 20 μL loop were used, that is, either a 5 mL silica column (BioZen dSEC-2 from Phenomenex) or a 24 mL Superdex column (S200 increase 10/300 from Cytiva).

Weight-average molar mass (noted M or M_{app}) of molecules passing through the SEC column is determined without column calibration by measuring at the maximum of the elution peak, their static light scattering at three angles (44°, 90°, and 136°), knowing their concentration c from UV and/or refractive index, by using the Zimm equation (Zimm, 1948):

$$\frac{Kc}{\Delta R_\theta} = \frac{1}{M_{app}} = \frac{1}{M} + 2A_2 c \quad (1)$$

with $K = \frac{4\pi^2 n_0^2}{\aleph_A \lambda^4}\left(\frac{\partial n}{\partial c}\right)^2$ and $\Delta R_\theta = R_{\theta,\text{sample}} - R_{\theta,\text{solvent}}$.

K is an optical constant, which depends on the refractive index (RI) of the buffer (n_0), the wavelength λ of the laser light (658 nm in the MiniDawn TREOS and Optilab T-rEX apparatus), the refractive index increment $\partial n/\partial c$ of the scattering molecule and $\aleph_A$ the Avogadro's number. θ is the angle between the incident and the scattered light. ΔR_θ is the excess Rayleigh ratio.

A_2 is the second virial coefficient, characterizing pairwise interaction forces between particles (e.g., PDC–PDC or detergent inter-micelle interactions), which can influence the value of the expected molar mass to a greater or lesser extent depending on the nature of the interactions. For attractive (*resp*. repulsive) interactions, A_2 is negative (*resp*. positive) and the apparent molar mass (M_{app}) will be higher (*resp*. lower) than expected.

For a PDC composed of a protein mass fraction (a) and a protein-bound detergent mass fraction (b), the concentration and molar mass of the complex are expressed as a function of the protein concentration and molar mass by:

$$c_{PDC} = (1+\delta)c_{MP} \quad (2)$$

$$M_{PDC} = (1+\delta)M_{MP} \quad (3)$$

with $\delta = b/a$, the bound detergent-to-protein mass ratio.

Considering that the PDC concentration is similar whatever the detector used (UV or RI), that is to say, $c_{PDC} = \frac{Abs_{280}}{\varepsilon_{PDC}} = \frac{dRI}{\partial n/\partial c_{PDC}}$, we can determine the mass ratio δ and the respective protein and bound detergent mass fractions a and b by the expressions:

$$\delta = \frac{dRI\varepsilon_{MP} - Abs_{280}\partial n/\partial c_{MP}}{Abs_{280}\partial n/\partial c_{Det} - dRI\varepsilon_{Det}} \quad (4)$$

$$a = \frac{1}{1+\delta} \text{ and } b = \frac{\delta}{1+\delta} \quad (5)$$

with Abs_{280} and dRI the measured absorbance at 280 nm and the differential refractive index of the complex, respectively, and ε_{MP}, ε_{Det}, $(\partial n/\partial c)_{MP}$ and $(\partial n/\partial c)_{Det}$, the respective extinction coefficients and RI increments of the protein and the detergent. The value of δ is then used to calculate ε_{PDC} and $\frac{\partial n}{\partial c_{PDC}}$ by applying the additivity rules for both absorbance and RI increment with:

$$\varepsilon_{PDC} = a\,\varepsilon_{MP} + b\,\varepsilon_{Det} \quad (6)$$

and

$$\frac{\partial n}{\partial c_{PDC}} = a\left(\frac{\partial n}{\partial c_{MP}}\right) + b\left(\frac{\partial n}{\partial c_{Det}}\right) \quad (7)$$

Finally, the inverse of the weight-average PDC molar mass is obtained by extrapolating the Zimm equation at zero angle.

An automatic procedure "*Protein Conjugate analysis*" from Astra (Wyatt Technology) permits the direct calculation of complex, detergent and protein

(apparent) molar masses, complex concentration, complex extinction coefficient (ε_{PDC}) and complex RI increment ($(\partial n/\partial c)_{PDC}$), using for ShuA $\varepsilon^{0.1\%} = 1.664$ L/g/cm at 280 nm and $\partial n/\partial c = 0.185$ mL/g and for both detergents, $\varepsilon^{0.1\%} \approx 0$ at 280 nm and $\partial n/\partial c = 0.141$ mL/g for DDM and $\partial n/\partial c = 0.123$ mL/g for OPOE, measured in their respective mobile phase, using the Optilab T-rEX refractometer. The methodology is thoroughly described in recent articles (Abel et al., 2021; Mégret-Cavalier et al., 2024; Zuniga et al., 2024).

In the case of a monomer/dimer equilibrium (mix) of ShuA–DDM complex, the respective fraction of monomer of complex, ϕ_{PDCM}, and dimer of complex, ϕ_{PDCD}, can be calculated from the parameters δ_{PDCmix}, $\frac{\partial n}{\partial c}_{PDCmix}$, ε_{PDCmix} and c_{PDCmix} obtained from the "Protein conjugate" module, knowing the values of ε_{MP}, ε_{Det}, $\frac{\partial n}{\partial c}_{MP}$, $\frac{\partial n}{\partial c}_{Det}$ (see details in Appendices S1 and S2) with the following equations:

$$\emptyset_{PDCM} = \frac{\frac{\varepsilon_{PDCmix}\delta_{PDCmix}}{\varepsilon_{MP}} - \frac{\delta_{PDCD}}{1+\delta_{PDCD}}}{\frac{\delta_{PDCM}}{1+\delta_{PDCM}} - \frac{\delta_{PDCD}}{1+\delta_{PDCD}}} \quad (8)$$

and

$$\emptyset_{PDCM} + \emptyset_{PDCD} = 1 \quad (9)$$

4.4 | In-line SEC-SAXS experiments on ShuA–detergent complexes

SAXS experiments on ShuA–detergent complexes (OPOE and DDM) were performed on the SWING beamline at the French synchrotron facility (SOLEIL, St-Aubin, France). With a wavelength of 1.033 Å and a sample-to-detector distance of 2 m, the achievable Q-range was 0.0036–0.5538 $Å^{-1}$, with $Q = 4\pi\sin\theta/\lambda$ and 2θ the scattering angle. ShuA sample in OPOE or DDM-containing buffer was injected through the same size exclusion columns as used for SEC-MALS on an Agilent HPLC system, which includes an automatic injector (5–100 µL), a UV–Vis cell to measure protein concentration at 280 nm, and the SAXS flow cell at a flow rate of 300 µL/min. For data reduction, buffer acquisition was performed at the beginning of the elution profile on the 5 mL-SEC column for 120 s with 180 frames and sample acquisition through peak elution for 380 s with 620 frames. When using a 24-mL SEC column, buffer acquisition was for 300 s with 300 frames and sample acquisition for 1700 s with 1033 frames. The 2D-SAXS patterns were normalized to the transmitted intensity and azimuthally averaged by using the Foxtrot program (Girardot & Viguier, 2015). Identical frames corresponding to elution buffer signal were averaged to provide a buffer signal for subtraction of individual sample frames. All SAXS analyses were done using BioXTAS RAW, an open-source software (Hopkins, 2024). Both forward intensity at $Q = 0$ ($I(0)$) and radius of gyration (R_G) were determined from the Guinier approximation $I(Q) = I(0)\exp.(-Q^2R_G{}^{2/3})$ at very small angles, assuming that $QR_G < 1.3$, and then were plotted as a function of sample frames in order to determine ranges of frames where the radius of gyration presents no significant variation. The forward intensity in absolute units is related to the PDC molar mass by the expression:

$$I(0) = \frac{cM}{\aleph_A} r_0^2 \left(\frac{n\aleph_A}{M} - \rho_s v\right)^2 \quad (10)$$

with c, M, n, v, respectively, the concentration, the molar mass, the number of electrons and the partial specific volume of the complex, $\aleph_A$ the Avogadro's number, ρ_s the electron scattering length densities of the solvent and r_0 the classical electron radius equal to 0.28179×10^{-12} cm/e^-.

For each injected sample, the averaged-subtracted intensity was normalized to the PDC concentration. A Guinier analysis allowed us to plot $S(c,0)$, the structure factor at $Q = 0$ as a function of PDC concentration, c, following the expression:

$$S(c,0) = \frac{I(c,0)}{I(0,0)} = 1 - 2MA_2c \quad (11)$$

A_2, the second virial coefficient, is positive for repulsive interactions and negative for attractive ones and is expressed in molmL/g. Conditions where the second virial coefficient is negative have long been known to favor crystallization of soluble and MPs (Berger et al., 2005; George & Wilson, 1994; Hitscherich et al., 2000).

4.5 | SANS experiments on ShuA–moDDM complex

The SANS measurements on ShuA in solution with moDDM were performed at the QUOKKA diffractometer (ANSTO, Sydney) and at D22 instrument (ILL, Grenoble, France). SANS measurements at QUOKKA (ANSTO, Sydney) were performed using neutrons with a wavelength of 6.0 Å and a wavelength spread of 10% (FWHM) at two sample-to-detector distances: 12 and 1.33 m. These settings covered q-ranges of 0.005–0.0592 and 0.00251–0.4896 $Å^{-1}$, respectively. Samples were placed in Hellma banjo suprasil quartz cuvettes of 1 mm thickness with a beam of 13 mm diameter.

SANS measurements at D22 (ILL, Grenoble) were performed using a wavelength of 6 Å ± 10%, a collimation length and central detector distance of 11.2 m, and

a second detector distance of 1.4 m. Samples were placed in Hellma rectangular cuvettes of 1 mm thickness, with a beam of 10 mm × 7 mm.

Data from both Quokka and D22 were reduced using Grasp software (Dewhurst, 2023), including transmission and thickness normalization, empty cell and blocked beam subtraction as well as calibration to absolutely scale by normalization with the direct beam intensity.

In both cases, 240 μL of ShuA at ca. 10 mg/mL purified in Tris HCl 20 mM pH 8, NaCl 100 mM, EDTA 1 mM, DDM-H_2O 0.5 mM was injected on a Superdex 200 increase 10/300 (24 mL column), pre-washed with pure D_2O and pre-equilibrated with Tris 50 mM, pD 7.5, NaCl 100 mM, moDDM 0.5 mM in 100% D_2O and then eluted at 150 μL/min to ensure optimal exchange of deuterated detergent around ShuA. Eluted fractions of ShuA (300 μL per fraction at ANSTO and 120 μL at ILL) were collected at the maximum of absorbance (ca. 2500 mAU) of the elution peak and the scattering signal was measured in a 1 mm thickness quartz cell. For the subsequent data reduction, the buffer flow-through from the column was collected, measured, and used for background subtraction.

4.6 | SAXS experiments on ShuA–moDDM/D_2O complex

The ShuA–moDDM/D_2O samples for SAXS experiments were prepared as for the SANS experiments: 200 μL of ShuA at ca. 10 mg/mL in 20 mM Tris HCl pH 8, 100 mM NaCl, 1 mM EDTA, 0.5 mM DDM/H_2O was injected onto a Superdex 200 increase 10/300, pre-washed with pure D_2O and pre-equilibrated with 50 mM Tris, pD 7.5, 100 mM NaCl, 0.5 mM moDDM in 100% D_2O and then eluted at 150 μL/min. Fractions of 150 μL were collected throughout the whole elution peak. The SAXS measurements on each fraction were performed in batch mode on the bioSAXS beamline BM29 at the European Synchrotron Radiation Facility (ESRF, Grenoble, France). The sample-detector distance was 2.812 m and the X-ray wavelength $\lambda = 0.992$ Å leading to a Q-range of 0.00628–0.5209 $Å^{-1}$. The beamline was equipped with a 2D detector (Pilatus3 2M) and an automated sample changer (Round et al., 2015). The sample storage and measurement temperatures were fixed at 20.0°C. To prevent radiation damage during the scattering experiments, data were collected in 10 successive 1 s frames, and the solution was moved in the capillary during exposure. All data manipulations were performed using a standard procedure via the ISPyB interface (Delagenière et al., 2011) and the program package PRIMUS (Konarev et al., 2003). All SAXS analyses were done using BioXTAS RAW. Forward intensity $I(0)$ and radius of gyration (R_G) of ShuA–moDDM/D_2O fractions were determined from Guinier analysis. The pair-distance distribution functions (PDDF) and the maximum particle dimensions (D_{max}) were determined by Inverse Fourier Transformation (IFT) of scattering intensity using the program GNOM (Svergun, 1992) from the ATSAS package.

4.7 | Crystallization experiment

Crystallization trials were tested with ShuA solubilized with DDM protocol and freshly purified in 50 mM Tris–HCl pH 7.5, 100 mM NaCl, 1 mM EDTA, 0.5 mM DDM. The crystallization was performed using the hanging-drop vapor-diffusion method (Linbro plate) by mixing 1 μL of ShuA-DDM at 5 mg/mL with 1 μL of crystallization solution (35% PEG 300, 100 mM NaCl, 100 mM Na-citrate pH 5). The reservoir volume was 1 mL and the incubation temperature 20°C. Crystals were observed by optical microscopy (Carl Zeiss SteREO Discovery V12 microscope).

AUTHOR CONTRIBUTIONS

A. Pozza: Investigation; writing – review and editing; resources; formal analysis; methodology. **A. Martel:** Resources; writing – review and editing; investigation. **M. Moir:** Writing – review and editing; investigation; resources. **T. A. Darwish:** Writing – review and editing; investigation; resources. **K. Wimalan:** Software; methodology. **A. Koutsioubas:** Writing – review and editing; software; methodology. **S. Combet:** Software; writing – review and editing; funding acquisition; methodology. **F. Bonneté:** Conceptualization; validation; supervision; writing – original draft; writing – review and editing; funding acquisition; project administration.

ACKNOWLEDGMENTS

This project received financial support from the CNRS through the CNRS-MITI interdisciplinary program "Modélisation du vivant" (2021–2022) and ANR through LABEX DYNAMO (ANR-11-LABX 0011). We acknowledge the framework CRISTECH-CNRS for financial support through an ITC (Initiative au Transfert Technologique) grant. We would like to warmly thank Dr. M. Budayova-Spano and Dr. S. Hjorth-Jensen for their welcome at IBS (Grenoble, France) for this ITC and for sharing their know-how and expertise in crystallization techniques. We also thank Dr. N. Dautin from LBPM at IBPC for the gift of the bacterial strain *E. coli* BL21 (DE3) Gold ΔABCF.

We gratefully acknowledge ESRF (Grenoble, France), SOLEIL (St Aubin, France), ILL (Grenoble, France) large-scale facilities for beamtime allocations on beamlines BM29 (BAG proposals MX-2456 and MX-2652) (Bonneté et al., 2026; Bonneté & Pozza, 2027), SWING (BAG proposal 20231081), D22 (proposal 9-13-1060) (Bonneté et al., 2023),

respectively. We acknowledge the support of the Australian Government in the provision of access to ANSTO's National Deuteration Facility which is partly funded through the National Collaborative Research Infrastructure Strategy (NCRIS) via NDF proposal DN13858. We thank local contacts, A. Popov and A. Calio (BM29), A. Thureau (Swing), A. Martel and L. Porcar (D22) and A. Whitten and K. Wood (QUOKKA) for their assistance during experiments. We also thank M. Sandroni, responsible for the ILL Chemistry Lab, as well as D. Wakeham and A. Duff (NDF-ANSTO) for technical assistance.

This work benefited from the use of the SasView application, originally developed under NSF award DMR-0520547. SasView contains code developed with funding from the European Union's Horizon 2020 research and innovation program under the SINE2020 project, grant agreement no. 654000.

DATA AVAILABILITY STATEMENT

The data that support the findings of this study are available from the corresponding author upon reasonable request.

ORCID

F. Bonneté https://orcid.org/0000-0002-1690-1757

REFERENCES

Abel S, Marchi M, Solier J, Finet S, Brillet K, Bonneté F. Structural insights into the membrane receptor ShuA in DDM micelles and in a model of gram-negative bacteria outer membrane as seen by SAXS and MD simulations. Biochim Biophys Acta (BBA). 2021;1863(2):183504. https://doi.org/10.1016/j.bbamem.2020.183504

Asakura S, Oosawa F. Interaction between particles suspended in solutions of macromolecules. J Polym Sci A. 1958;33(126):183–92. https://doi.org/10.1002/pol.1958.1203312618

Barret L-A, Barrot-Ivolot C, Raynal S, Jungas C, Polidori A, Bonneté F. Influence of hydrophobic micelle structure on crystallization of the photosynthetic RC-LH1-PufX complex from *Rhodobacter blasticus*. J Phys Chem B. 2013;117(29):8770–81. https://doi.org/10.1021/jp403483q

Berger BW, Gendron CM, Robinson CR, Kaler EW, Lenhoff AM. The role of protein and surfactant interactions in membrane-protein crystallization. Acta Cryst D. 2005;61:724–30. https://doi.org/10.1107/S0907444904029063

Birch J, Cheruvara H, Gamage N, Harrison PJ, Lithgo R, Quigley A. Changes in membrane protein structural biology. Biology. 2020;9(11):401. https://doi.org/10.3390/biology9110401

Bonneté F, Pozza A. From structure to drug design. Grenoble, France: ESRF; 2027. https://doi.org/10.15151/ESRF-ES-1830135339

Bonneté F, Finet S, Tardieu A. Second virial coefficient: variations with lysozyme crystallization conditions. J Crystal Growth. 1999;196:403–14. https://doi.org/10.1016/S0022-0248(98)00826-4

Bonneté F, Combet S, Martel A, Porcar L, Pozza A. SASMod: a new methodological approach for ShuA–DDM complex structure modeling. Grenoble, France: ILL; 2023. https://doi.org/10.5291/ILL-DATA.9-13-1060

Bonneté F, Pozza A, Saade C. From structure to drug design. Grenoble, France: ESRF; 2026. https://doi.org/10.15151/ESRF-ES-1118672762

Breyton C, Tribet C, Olive J, Dubacq JP, Popot JL. Dimer to monomer conversion of the cytochrome b6 f complex. Causes and consequences. J Biol Chem. 1997;272(35):21892–900. https://doi.org/10.1074/jbc.272.35.21892

Brillet K, Meksem A, Thompson A, Cobessi D. Expression, purification, crystallization and preliminary X-ray diffraction analysis of the TonB-dependent haem outer membrane transporter ShuA from shigella dysenteriae. Acta Cryst F. 2009;65(Pt 4):402–5. https://doi.org/10.1107/S1744309109008148

Chien C-T, Maduke M, Chiu W. Single-particle cryogenic electron microscopy structure determination for membrane proteins. Curr Opin Struct Biol. 2025;92:103047. https://doi.org/10.1016/j.sbi.2025.103047

Choy BC, Cater RJ, Mancia F, Pryor EE. A 10-year meta-analysis of membrane protein structural biology: detergents, membrane mimetics, and structure determination techniques. Biochim Biophys Acta (BBA). 2021;1863(3):183533. https://doi.org/10.1016/j.bbamem.2020.183533

Cleveland TE, He W, Evans AC, Fischer NO, Lau EY, Coleman MA, et al. Small-angle X-ray and neutron scattering demonstrates that cell-free expression produces properly formed disc-shaped nanolipoprotein particles. Protein Sci. 2018;27(3):780–9. https://doi.org/10.1002/pro.3365

Cobessi D, Meksem A, Brillet K. Structure of the heme/hemoglobin outer membrane receptor ShuA from shigella dysenteriae: heme binding by an induced fit mechanism. Proteins Struct Funct Bioinform. 2010;78(2):286–94. https://doi.org/10.1002/prot.22539

Combet S, Bonneté F, Finet S, Pozza A, Saade C, Martel A, et al. Effect of amphiphilic environment on the solution structure of mouse TSPO translocator protein. Biochimie. 2023;205:61–72. https://doi.org/10.1016/j.biochi.2022.11.014

Delagenière S, Brenchereau P, Launer L, Ashton AW, Leal R, Veyrier S, et al. ISPyB: an information management system for synchrotron macromolecular crystallography. Bioinformatics. 2011;27:3186–92. https://doi.org/10.1093/bioinformatics/btr535

Dewhurst CD. Graphical reduction and analysis small-angle neutron scattering program: GRASP. J Appl Cryst. 2023;56(5):1595–609. https://doi.org/10.1107/s1600576723007379

Fisher LE, Engelman DM, Sturgis JN. Effect of detergents on the Association of the Glycophorin a Transmembrane Helix. Biophys J. 2003;85(5):3097–105. https://doi.org/10.1016/S0006-3495(03)74728-6

Fleming KG. Standardizing the free energy change of transmembrane helix–helix interactions. J Mol Biol. 2002;323(3):563–71. https://doi.org/10.1016/s0022-2836(02)00920-8

Franke D, Svergun DI. DAMMIF, a program for rapid ab-initio shape determination in small-angle scattering. J Appl Cryst. 2009;42(2):342. https://doi.org/10.1107/S0021889809000338

García-Nafría J, Tate CG. Structure determination of GPCRs: cryo-EM compared with X-ray crystallography. Biochem Soc Trans. 2021;49(5):2345–55. https://doi.org/10.1042/bst20210431

Gelbart WM, Ben-Shaul A, McMullen WE, Masters A. Micellar growth due to interaggregate interactions. J Phys Chem. 1984;88(5):861–6. https://doi.org/10.1021/j150649a008

George A, Wilson WW. Predicting protein crystallization from a dilute solution property. Acta Cryst D. 1994;50:361–5. https://doi.org/10.1107/S0907444994001216

Girardot R, Viguier G. FOXTROT: A JAVA-Based Application to Reduce and Analyse SAXS and WAXS Piles of 2D Data at Synchrotron Soleil. canSAS-VIII, Tokai, Japan. 2015.

Giubertoni G, Bonn M, Woutersen S. D_2O as an imperfect replacement for H_2O: problem or opportunity for protein research? J Phys Chem B. 2023;127(38):8086–94. https://doi.org/10.1021/acs.jpcb.3c04385

Glatter O, Kratky O. Small angle X-ray scattering. London, New York: Academic Press; 1982. ISBN:978-0-12-286280-9.

Grant TD. Ab initio electron density determination directly from solution scattering data. Nat Methods. 2018;15(3):191–3. https://doi.org/10.1038/nmeth.4581

Guan L. The rapid developments of membrane protein structure biology over the last two decades. BMC Biol. 2023;21(1):300. https://doi.org/10.1186/s12915-023-01795-9

Guo Y. Be cautious with crystal structures of membrane proteins or complexes prepared in detergents. Crystals. 2020;10(2):86. https://doi.org/10.3390/cryst10020086

Haidar Y, Konermann L. Effects of hydrogen/deuterium exchange on protein stability in solution and in the gas phase. J Am Soc Mass Spectrometry. 2023;34(7):1447–58. https://doi.org/10.1021/jasms.3c00130

Healey RD, Basu S, Humm AS, Leyrat C, Cong X, Golebiowski J, et al. An automated platform for structural analysis of membrane proteins through serial crystallography. Cell Reports Methods. 2021;1(6):100102. https://doi.org/10.1016/j.crmeth.2021.100102

Heuberger EH, Veenhoff LM, Duurkens RH, Friesen RH, Poolman B. Oligomeric state of membrane transport proteins analyzed with blue native electrophoresis and analytical ultracentrifugation. J Mol Biol. 2002;317(4):591–600. https://doi.org/10.1006/jmbi.2002.5416

Hitscherich C, Kaplan J, Allaman M, Wiencek J, Loll PJ. Static light scattering studies of OmpF porin: implications for integral membrane protein crystallization. Protein Sci. 2000;9(8):1559–66. https://doi.org/10.1110/ps.9.8.1559

Hopkins J. BioXTAS RAW 2: new developments for a free open-source program for small-angle scattering data reduction and analysis. J Appl Cryst. 2024;57(1):194–208. https://doi.org/10.1107/S1600576723011019

Jia Y, Narayanan J, Liu XY, Liu Y. Investigation on the mechanism of crystallization of soluble protein in the presence of nonionic surfactant. Biophys J. 2005;89(6):4245–51. https://doi.org/10.1529/biophysj.105.066449

Kaufmann TC, Engel A, Rémigy HW. A novel method for detergent concentration determination. Biophys J. 2006;90(1):310–7. https://doi.org/10.1529/biophysj.105.070193

Konarev PV, Volkov VV, Sokolova AV, Koch MHJ, Svergun DI. PRIMUS: a windows PC-based system for small-angle scattering data analysis. J Appl Cryst. 2003;36:1277–82.

Koutsioubas A, Jaksch S, Pérez J. DENFERT version 2: extension of ab initio structural modelling of hydrated biomolecules to the case of small-angle neutron scattering data. J Appl Cryst. 2016;49(2):690–5. https://doi.org/10.1107/S1600576716003393

Kulkarni AM, Chatterjee AP, Schweizer KS, Zukoski CF. Effects of polyethylene glycol on protein interactions. J Chem Phys. 2000;113(21):9863–73. https://doi.org/10.1063/1.1321042

Lang P, Glatter O. Small-angle X-ray scattering from aqueous solutions of tetra(oxyethylene)-n-octyl ether. Langmuir. 1996;12(5):1193–8. https://doi.org/10.1021/la9507646

Lee S, Mao A, Bhattacharya S, Robertson N, Grisshammer R, Tate CG, et al. How do short chain nonionic detergents destabilize G-protein-coupled receptors? J Am Chem Soc. 2016;138(47):15425–33. https://doi.org/10.1021/jacs.6b08742

Marenduzzo D, Finan K, Cook PR. The depletion attraction: an underappreciated force driving cellular organization. J Cell Biol. 2006;175(5):681–6. https://doi.org/10.1083/jcb.200609066

Mégret-Cavalier M, Pozza A, Cece Q, et al. Starting with an Integral Membrane Protein Project for Structural Biology: Production, Purification, Detergent Quantification, and Buffer Optimization-Case Study of the Exporter CntI from *Pseudomonas aeruginosa*. Bacterial Secretion Systems (MIMB). Cham: Springer Nature; 2024. https://doi.org/10.1007/978-1-0716-3445-5_261064-3745

Meuskens I, Michalik M, Chauhan N, Linke D, Leo JC. A new strain collection for improved expression of outer membrane proteins. Front Cell Infect Microbiol. 2017;7:464. https://doi.org/10.3389/fcimb.2017.00464

Midtgaard SR, Darwish TA, Pedersen MC, Huda P, Larsen AH, Jensen GV, et al. Invisible detergents for structure determination of membrane proteins by small-angle neutron scattering. FEBS. 2018;285(2):357–71. https://doi.org/10.1111/febs.14345

Molodenskiy DS, Mertens HDT, Svergun DI. An automated data processing and analysis pipeline for transmembrane proteins in detergent solutions. Sci Rep. 2020;10(1):8081. https://doi.org/10.1038/s41598-020-64933-1

Newstead S, Ferrandon S, Iwata S. Rationalizing {alpha}-helical membrane protein crystallization. Protein Sci. 2008;17(3):466–72. https://doi.org/10.1110/ps.073263108

Perez J, Koutsioubas A. Memprot: a program to model the detergent corona around a membrane protein based on SEC-SAXS data. Acta Cryst D. 2015;71:86–93. https://doi.org/10.1107/s1399004714016678

Pocanschi CL, Kleinschmidt JH. The thermodynamic stability of membrane proteins in micelles and lipid bilayers investigated with the Ferrichrom receptor FhuA. J Membr Biol. 2022;255(4):485–502. https://doi.org/10.1007/s00232-022-00238-w

Polidori A, Raynal S, Barret LA, Dahani M, Barrot-Ivolot C, Jungas C, et al. Sparingly fluorinated maltoside-based surfactants for membrane-protein stabilization. New J Chem. 2016;40:5364–78. https://doi.org/10.1039/C5NJ03502C

Ray D, Kumar S, Aswal VK, Kohlbrecher J. Tuning nanoparticle–micelle interactions and resultant phase behavior. Langmuir. 2018;34(1):259–67. https://doi.org/10.1021/acs.langmuir.7b03429

Reslan M, Kayser V. The effect of deuterium oxide on the conformational stability and aggregation of bovine serum albumin. Pharm Dev Technol. 2018;23(10):1030–6. https://doi.org/10.1080/10837450.2016.1268157

Rosenbusch JP, Lustig A, Grabo M, Zulauf M, Regenass M. Approaches to determining membrane protein structures to high resolution: do selections of subpopulations occur? Micron. 2001;32(1):75–90. https://doi.org/10.1016/s0968-4328(00)00021-4

Round A, Felisaz F, Fodinger L, Gobbo A, Huet J, Villard C, et al. BioSAXS sample changer: a robotic sample changer for rapid and reliable high-throughput X-ray solution scattering experiments. Acta Cryst D. 2015;71(1):67–75. https://doi.org/10.1107/s1399004714026959

Schrodinger LLC. The PyMOL Molecular Graphics System, Version 1.8. 2015.

Spinozzi F, Gazzillo D, Giacometti A, Mariani P, Carsughi F. Interaction of proteins in solution from small-angle scattering: a perturbative approach. Biophys J. 2002;82(4):2165–75. https://doi.org/10.1016/S0006-3495(02)75563-X

Stetsenko A, Guskov A. An overview of the top ten detergents used for membrane protein crystallization. Crystals. 2017;7(7):197. https://doi.org/10.3390/cryst7070197

Sumner J, Qian S. DENSS-multiple: a structure reconstruction method using contrast variation of small-angle neutron scattering based on the DENSS algorithm. BBA Adv. 2022;2:100063. https://doi.org/10.1016/j.bbadva.2022.100063

Sun J, Kulandaisamy A, Liu J, Hu K, Gromiha MM, Zhang Y. Machine learning in computational modelling of membrane protein sequences and structures: from methodologies to applications. Comput Struct Biotechnol J. 2023;21:1205–26. https://doi.org/10.1016/j.csbj.2023.01.036

Svergun DI. Determination of the regularization parameter in indirect-transform methods using perceptual criteria. J Appl Cryst. 1992;25:495–503.

Svergun DI. Restoring low resolution structure of biological macromolecules from solution scattering using simulated annealing. Biophys J. 1999;76(6):2879–86. https://doi.org/10.1016/S0006-3495(99)77443-6

Svergun DI, Richard S, Koch MHJ, Sayers Z, Kuprin S, Zaccai G. Protein hydration in solution: experimental observation by X-ray and neutron scattering. PNAS. 1998;95(5):2267–72. https://doi.org/10.1073/pnas.95.5.2267

Tamm LK, Hong H, Liang B. Folding and assembly of β-barrel membrane proteins. Biochim Biophys Acta. 2004;1666(1):250–63. https://doi.org/10.1016/j.bbamem.2004.06.011

Tanford C. The hydrophobic effect: formation of micelles and biological membranes. New York: John Wiley & Sons, Inc; 1980 1543-0472.

Tate CG. Practical considerations of membrane protein instability during purification and crystallisation. Heterologous Expression of Membrane Proteins. Chapter 12. Cham: Springer Nature; 2010. https://doi.org/10.1007/978-1-60761-344-2_12978-1-4939-6132-0

Tulumello D, Deber C. Effciency of detergents at maintaining membrane protein structures in their biologically relevant forms. Biochim Biophys Acta (BBA). 2012;1818:1351–8. https://doi.org/10.1016/j.bbamem.2012.01.013

Urner LH, Junge F, Fiorentino F, el-Baba TJ, Shutin D, Nölte G, et al. Rationalizing the optimization of detergents for membrane protein purification. Chemistry. 2023;29(30):e202300159. https://doi.org/10.1002/chem.202300159

Valadez-Perez N, Liu Y, Castañeda-Priego R. Cluster morphology of colloidal systems with competing interactions. Front Phys. 2021; 9:637138. https://doi.org/10.3389/fphy.2021.637138

Volkov VV, Svergun DI. Uniqueness of ab initio shape determination in small-angle scattering. J Appl Cryst. 2003;36(3 Part 1):860–4. https://doi.org/10.1107/S0021889803000268

Wolfe AJ, Parella KJ, Movileanu L. High-throughput screening of protein–detergent complexes using fluorescence polarization spectroscopy. Curr Protoc Protein Sci. 2019;97(1):e96. https://doi.org/10.1002/cpps.96

Woubshete M, Cioccolo S, Byrne B. Advances in membrane mimetic systems for manipulation and analysis of membrane proteins: detergents, polymers, lipids and scaffolds. ChemPlusChem. 2024;89(6):e202300678. https://doi.org/10.1002/cplu.202300678

Yang Z, Wang C, Zhou Q, An J, Hildebrandt E, Aleksandrov LA, et al. Membrane protein stability can be compromised by detergent interactions with the extramembranous soluble domains. Protein Sci. 2014;23(6):769–89. https://doi.org/10.1002/pro.2460

Yin H, Flynn AD. Drugging membrane protein interactions. Annu Rev Biomed Eng. 2016;18:51–76. https://doi.org/10.1146/annurev-bioeng-092115-025322

Yoon S, Bae HE, Hariharan P, Nygaard A, Lan B, Woubshete M, et al. Rational approach to improve detergent efficacy for membrane protein stabilization. Bioconjug Chem. 2024;35(2):223–31. https://doi.org/10.1021/acs.bioconjchem.3c00507

Zampieri V, Hilpert C, Garnier M, Gestin Y, Delolme S, Martin J, et al. The det.Belt server: a tool to visualize and estimate amphipathic solvent belts around membrane proteins. Membranes. 2021; 11(7):459. https://doi.org/10.3390/membranes11070459

Zhang F, Skoda MWA, Jacobs RMJ, Martin RA, Martin CM, Schreiber F. Protein interactions studied by SAXS: effect of ionic strength and protein concentration for BSA in aqueous solutions. J Phys Chem B. 2007;111(1):251–9. https://doi.org/10.1021/jp0649955

Zhang F, Roosen-Runge F, Sauter A, et al. The role of cluster formation and metastable liquid—liquid phase separation in protein crystallization. Faraday Discuss. 2012;159:313. https://doi.org/10.1039/C2FD20021J

Zimm BH. The scattering of light and the radial distribution function of high polymer solutions. J Chem Physics. 1948;16(12):1093–9. https://doi.org/10.1063/1.1746738

Zulauf M, Weckstrom K, Hayter JB, Degiorgio V, Corti M. Neutron scattering study of micelle structure in isotropic aqueous solutions of poly(oxyethylene) amphiphiles. J Phys Chem. 1985; 89(15):3411–7. https://doi.org/10.1021/j100261a051

Zuniga D, Zoumpoulakis A, Veloso RF, Peverini L, Shi S, Pozza A, et al. Biochemical, biophysical, and structural investigations of two mutants (C154Y and R312H) of the human Kir2.1 channel involved in the Andersen-Tawil syndrome. FASEB J. 2024;38: e70146. https://doi.org/10.1096/fj.202401567R

SUPPORTING INFORMATION

Additional supporting information can be found online in the Supporting Information section at the end of this article.

How to cite this article: Pozza A, Martel A, Moir M, Darwish TA, Wimalan K, Koutsioubas A, et al. Unraveling ShuA detergent-induced colloidal behavior in solution: A comprehensive SEC-MALS, SAXS, and SANS study. Protein Science. 2025;34(9):e70258. https://doi.org/10.1002/pro.70258